CHALMERS

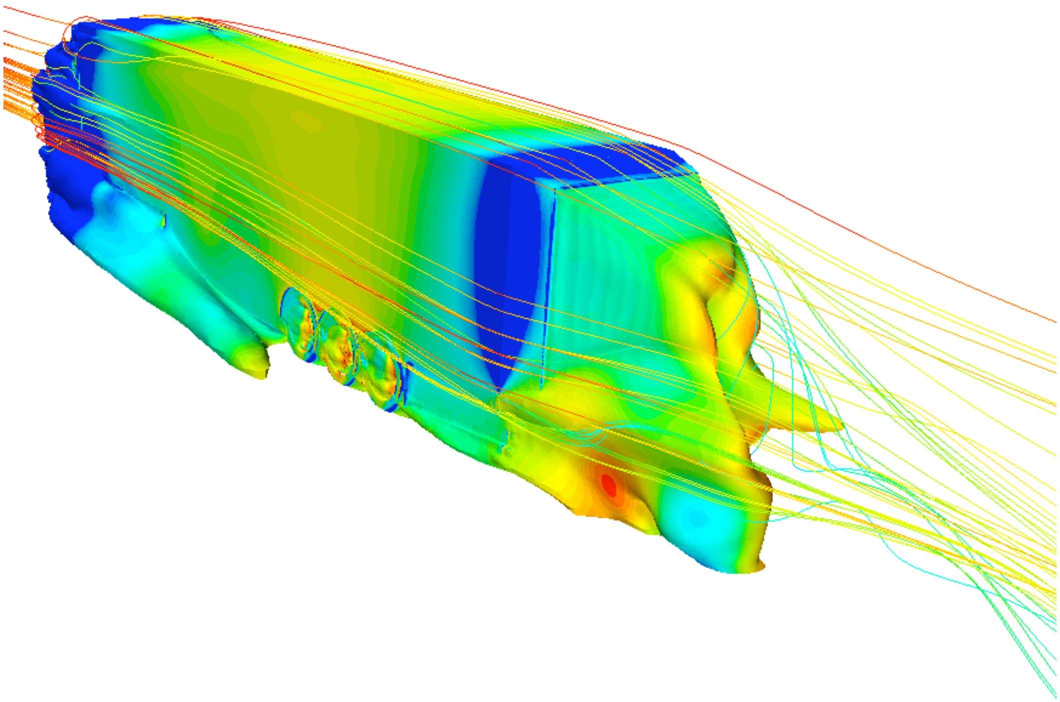

CFD Analysis of Aerodynamic Trailer Devices for Drag Reduction of Heavy Duty Trucks

Master's Thesis in the Master's programme Automotive Engineering

CHRISTOFFER HÅKANSSON

MALIN J. LENNGREN

Department of Applied Mechanics
Division of Vehicle Engineering and Autonomous Systems
CHALMERS UNIVERSITY OF TECHNOLOGY
Göteborg, Sweden 2010

Master's Thesis 2010:10

MASTER'S THESIS 2010:10

CDF Analysis of Aerodynamic Trailer Devices for Drag Redution of Heavy Duty Trucks

Master's thesis in the Master's programme of Automotive Engineering

CHRISTOFFER HÅKANSSON

MALIN J. LENNGREN

Department of Applied Mechanics
Division of Vehicle Engineering and Autonomous Systems
CHALMERS UNIVERSITY OF TECHNOLOGY
Göteborg, Sweden 2010

CFD Analysis of Aerodynamic Trailer Devices for Drag Reduction of Heavy Duty Trucks

Master's thesis in the Master's programme of Automotive Engineering

CHRISTOFFER HÅKANSSON

MALIN J. LENNGREN

Master's Thesis 2010:10
ISSN 1652-8557
Department of Applied Mechanics
Division of Vehicle Engineering and Autonomous Systems
Chalmers University of Technology
SE-412 96 Göteborg
Sweden
Telephone: + 46 (0)31-772 1000

Cover:
Pressure coefficient displayed on an iso surface of total pressure equal zero, together with streamlines colored by the velocity magnitude.

Chalmers Reproservice / Department of Applied Mechanics
Göteborg, Sweden 2010

CFD Analysis of Aerodynamic Trailer Devices for Drag Reduction of Heavy Duty Trucks

Master's thesis in the Master's programme of Automotive Engineering
CHRISTOFFER HÅKANSSON
MALIN J. LENNGREN
Department of Applied Mechanics
Division of Vehicle Engineering and Autonomous Systems
Chalmers University of Technology

ABSTRACT

Today's demand of reducing the fuel consumption of vehicles is one of the most challenging issues within the automotive industry. Together with the increased fuel price, the development of more fuel efficient vehicles has escalated. A recent research about fuel reduction technologies for trucks showed that aerodynamic improvement is one of the most important technologies when it comes to fuel saving.

Volvo Trucks has a well established aerodynamic focus in the product development process of the tractor, although there are no focus on trailer aerodynamics. Therefore, more research of aerodynamics around the tractor and the trailer is desirable to see the possibilities to further reduce drag.

Different aerodynamic trailer devices and aerodynamically shaped trailers have been tested by means of Computational Fluid Dynamics, in order to investigate their influence on the flow around the truck. The tests were simulated with a speed of 90 km/h, and with yaw angles of 0° and 5°. In addition, drag contribution from different regions was analyzed to see where it is possible to gain most drag. Finally, an evaluation was done to see if the results from the simulations could promote any possible aerodynamic profits of a mutual development between tractor and trailer manufacturers.

The results show that the largest effects of the trailer devices are achieved during 5° yaw, this especially applies for the undercarriage treatment. Furthermore, devices that were implemented in the undercarriage and base region presented the best results, which indicates that these regions are most susceptible for drag improvements. However, it was very difficult to achieve a balanced base wake; devices placed at the rear face of the trailer improved the flow from the roof and the upper sides, whereas the air at ground level was very difficult to affect due to a disturbed undercarriage flow. The gap treatment improved the flow over the gap and along the trailer roof, although a larger gap clearance would probably have amplified the effect of these devices.

Furthermore, this project has shown the importance of integrating the tractor and trailer development for further aerodynamic improvements. Profits of such mutual development can for example be that the gap could be further reduced, and the interface and flow transition between the cab, the trailer, the tractor chassis and the trailer undercarriage can be optimized.

Key words: aerodynamics CFD drag reduction trailer device STARCCM+ truck

Contents

Preface

This master's thesis has investigated how different aerodynamic trailer devices and aerodynamic trailer shapes affect the flow around a truck. This project also includes an evaluation of possible aerodynamic profits of a common development between tractor and trailer manufactures. The project has been carried out from January 2010 to June 2010.

The thesis has been performed at Volvo 3P and we would like to take the opportunity to thank Volvo 3P for giving us the good fortune to work with such an interesting topic and further develop our skills within aerodynamics and CFD. Many employees at Volvo 3P has contributed with help and support that we highly appreciate, although there are a few persons that we especially would like to acknowledge. We would like to express our sincere gratitude to Zenitha Chronéer *Ph.D* Analysis engineer CFD, our supervisor at Volvo 3P, for her help, support and expertise during this project. Furthermore, many thanks to Helena Martini, our supervisor at Chalmers University of Technology, and Linus Hjelm, aerodynamicist at Volvo 3P, for greatly appreciated guidance and feedback. We would also like to thank our examiner Professor Lennart Löfdahl for supporting and believing in us.

Finally, we would like to thank group 26547 at Volvo 3P for contributing to an amiable and positive working environment.

Göteborg June 2010

Christoffer Håkansson and Malin J. Lenngren

Notations

A	Vehicle frontal area $\left[m^2\right]$
C_d	Drag coefficient $[-]$
$C_{d-weighted}$	Weighted drag coefficient $[-]$
C_{d-0deg}	Drag coefficient in 0° yaw $[-]$
C_{d-5deg}	Drag coefficient in 5° yaw $[-]$
ΔC_d	Difference in drag between the specific case and the reference $[-]$
ρ	Density $\left[kg/m^3\right]$
F_{drag}	Drag force $[N]$
F_{roll}	Rolling resistance $[N]$
V	Velocity $[m/s]$
V_x	Velocity in 0° yaw $[m/s]$
$V_{cross-wind}$	Velocity in 5° yaw $[m/s]$
t	Time $[s]$
p	Pressure $[Pa]$
μ	Viscosity $[kg/m \cdot s]$
g	Gravity $\left[m/s^2\right]$
c_p	Specific heat capicity $[J/kg \cdot K]$
T	Temperature C°
k	Coefficient of thermal conductivity $[W/K \cdot m]$
Φ	Viscous dissipation function $[-]$
$y+$	Dimensionless wall distance $[-]$

Abbreviations

CAD	Computer Aided Design
CFD	Computational Fluid Dynamics
DC	Drag Counts
DNS	Direct Numerical Simulation
FS	Fuel Saving
LBM	Lattice Boltzmann Method
LES	Large Eddy Simulation
PID	Property Identification
$RANS$	Reynolds Averaged Navier-Stoke

1 Introduction

One of the most important environmental issues within the automotive industry today is to reduce the fuel consumption and emissions. Together with the increased fuel price this has resulted in a "green race" within automotive companies in order to stay competitive, and the development of fuel efficient products has escalated. This is, among other methods, achieved by improving efficiency of the engine, reducing rolling resistance and improving aerodynamics. A recent project called OptiFuel, conducted by Renault Trucks, contains an investigation of new technologies to reduce the fuel consumption. The report states that aerodynamic improvements of the tractor unit and the semi-trailer, and thereby drag reduction, is one of the most important issues when it comes to fuel saving [2].

Figure 1 shows the required power to overcome aerodynamic drag and rolling resistance as a function of speed for a truck of 40 tons. As seen in the picture, there is a cubic increase of drag, whereas the rolling resistance grows linearly with speed. Above approximately 80 km/h the aerodynamic drag becomes dominating, which makes aerodynamics very important for long-distance transport where speeds up to 90 km/h is common. However, it should be mentioned that aerodynamic drag is still important below this speed, although not to the same extent. By reducing drag, less power is needed and fuel consumption can be reduced.

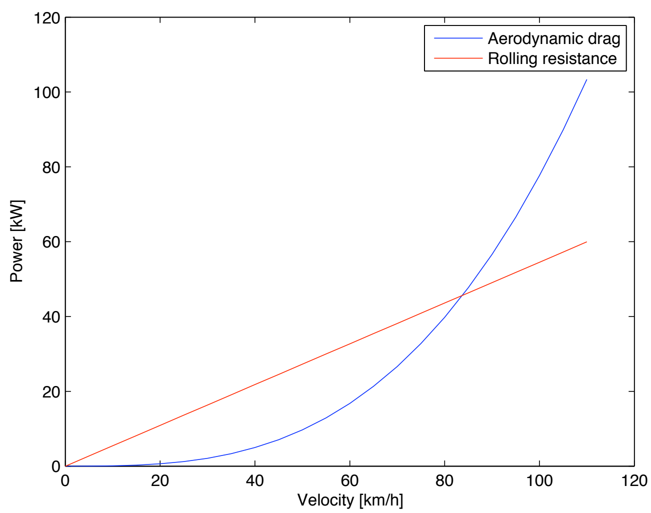

Figure 1: Aerodynamic drag versus Rolling resistance for a truck with a C_d of 0.5, $frontal\ area = 10.2\,m^2$ and a rolling resistance coefficient set to 0.005

Throughout this report the word tractor refers to the tractor unit, including chassis, cab, wheels and engine. Truck is used when referring to both the tractor unit and the semi-trailer. Semi-trailer is henceforth abbreviated to trailer.

1.1 Project Background

Today's topic of environmental issues forces companies like Volvo Trucks to constantly improve the fuel efficiency and the emissions. The aerodynamic focus in the product development process of the tractor is today well established and substantial research has been made in order to optimize the drag. Different types of roof deflectors, side deflectors and chassis fairings are just a few good examples of aerodynamic improvements that have made it possible to reduce the fuel consumption. However, there are many different factors that need to be considered when designing a tractor, for example brand identity and legislation, further adjustments to design the tractor aerodynamically are therefore limited. According to experts at Volvo, adjustments on the tractor today, can in best-case scenario give a drag improvement of up to 1 or 2 %.

Since Volvo only produces tractors, all resources are focused on the tractor only, and no valuable assets such as time, knowledge and money is spent on the trailer. When optimizing the tractor aerodynamically at Volvo, a standard box trailer without modifications is used and knowledge of how the tractor is functioning aerodynamically with other types of trailers or with modified box trailers is limited. In addition, the communication between Volvo and trailer manufacturers is lacking, which has retarded the integration of the tractor and trailer in order to reduce drag. Regarding Volvo's goal of improving the fuel efficiency by 1% each year [6], it could be beneficial to consider the whole combination tractor and trailer in the continuing work of aerodynamic development.

On today's market there exist different trailer shapes and several types of trailer devices to reduce drag, although they are not very commonly used on the roads. Some of these are add-on devices, developed by independent companies, which can be added after purchase. It is also possible to acquire an already aerodynamically shaped trailer, a so-called teardrop trailer. A British trailer manufacture claims that their teardroped-shaped trailer gives 10 % in fuel saving [7].

1.2 Objectives

The aim of this project is to investigate how the flow around a Volvo FH-tractor and a trailer is influenced by drag reducing trailer devices, and to see how much it is possible to reduce drag. Additionally, the ambition is to obtain an understanding of drag contribution from different areas around the truck, and to see where it is possible to gain most drag reduction. Finally, this project will also include a short evaluation of possible aerodynamic profits of a mutual development of the tractor and the trailer.

1.3 Procedure

This project starts with a research of existing trailer devices. The research will investigate what type of drag reducing devices that are used on trailers today and how they work. In consultation with supervisor, CAD-models of some of these devices together with own suggestions will be generated. The devices will then be tested, compared and evaluated by means of Computational Fluid Dynamics (CFD) in order to acquire an understanding of the flow field around the truck and how combinations of the devices can improve drag even more. The procedure and case setup will be further explained in Chapter 3.

1.4 Delimitations

This project does not consider any costs of either production or implementation of the devices. The devices are only aerodynamically evaluated and choice of material and applicability are not discussed. Furthermore, no consideration is taken to legislation about length of the trailer with added devices.

Due to time limitation only a restricted number of devices are tested and evaluated to verify their efficiency. Optimization of the devices is not included in this thesis. The devices are added on a standard box trailer together with a Volvo FH-H2 model. No modifications are done on the tractor.

The CFD settings used in this thesis are recommended by Volvo and evaluation of how different settings would affect the result is not included in this project.

2 Theory

In this chapter the general basics of aerodynamics around a truck are explained together with some of the existing drag reducing devices. Furthermore, a brief introduction is given to fluid dynamics and the tool used in this project, Computational Fluid Dynamics (CFD).

2.1 Truck aerodynamics

Aerodynamic drag consists of two components, pressure drag (force acting normal to surface) and friction drag (force acting tangential to surface). Friction drag is due to shear stress between the fluid and the surface, whereas pressure drag is due to a pressure difference between the front and the rear of the body. For a truck, and other blunt bodies, the pressure drag is the most dominating one and contributes to more than 90 percent of the total drag [15]. In addition to the tractor front, the regions that represent the main drag-contributing areas around a truck are: the gap between the tractor and the trailer, the base wake behind the trailer and the undercarriage [11].

2.1.1 Tractor-trailer gap

The effect of the gap clearance between the tractor and the trailer is very much dependent on how large the gap is. One of the drag contributing issues with the larger gaps is that air goes into the gap and hits the trailer front, which results in an increased pressure drag. This pressure becomes even greater if there is a height difference between the tractor and the trailer. If this is the situation it is beneficial to use a roof deflector with an angle adjusted to the height of the trailer. During cross-wind conditions more air is entering the gap which will increase the flow separation, and thereby turbulence, on the leeward side of the trailer. This will affect the drag and stability.

In order to reduce the drag due to the gap clearance there exist several different solutions of aerodynamic devices which can be implemented on the truck. Most common is the roof deflector and the side deflectors added on the tractor to guide the air over the gap. For those configurations where the gap is large, there are a number of devices to improve the aerodynamics. The main purpose of such devices, added on the trailer front, is to prevent uncontrolled circulation and cross-flow in the gap, improve the flow over the gap and to reduce the pressure acting on the trailer. Cross-flow vortex trap and Nose cone, seen in Figure 2, are two examples of how aerodynamic trailer devices can be implemented in the gap. The Cross-flow vortex trap device is aiming at creating a couple of stable vortices at the trailer front in order to reduce the pressure in this region. The Nose cone is used to improve the flow over the gap and to reduce the pressure on the trailer front. Full-scale wind-tunnel tests conducted at the National Research Council of Canada (NRC), performed with a speed of 100 km/h and over a yaw sweep to calculate the wind average, states that these devices reduce drag by 2 and 34 drag counts, respectively (information about drag counts is found in Subchapter 3.3) [9]. As can be seen in the pictures these results are achieved when the gap clearance is fairly large.

Figure 2: Gap treatment: Cross-flow vortex trap and Nose cone [9]

2.1.2 Undercarriage

The undercarriage flow encounters a large amount of disturbances due to irregular geometries with sharp edges underneath the tractor and the trailer. Together with other disturbances, such as rotating wheels, this results in a reduction of velocity in the flow, so-called low-momentum flow, under the trailer with numerous separations and energy losses.

Different types of devices placed under the trailer can be used to improve the undercarriage flow by directing the flow along the side of the trailer, see Figure 3. This is even more beneficial during cross-wind conditions since it prevents cross-flows. Different types of side skirts have demonstrated a drag reduction of up to 48 drag counts [9]. Bogey trailer fairing is another undercarriage treatment that is used to reduce disturbances as the air hits the trailer bogey, see Figure 3. A smoother trailer bottom with less irregularity can also be a good adjustment to improve the undercarriage flow.

Figure 3: Undercarriage treatment: Side skirts and Bogey wheel fairing [9]

2.1.3 Rear of the trailer

At the rear of the trailer a dominant base wake is created, containing unsteady turbulent flow. This is a result of a low-momentum flow along the top and the sides of the trailer that separates at the trailing edge of the trailer. The low-momentum flow from the undercarriage interacts with the base wake, resulting in an even greater turbulent base flow. A consequence of this is a low-pressure region that is created behind the trailer that contributes to drag.

There exist different types of aerodynamic devices to decrease and stabilize the base wake by guiding the flow at the rear of the trailer. By extending the rear with different types of angled plates, the flow attachment is maintained and the air can be guided into the center of the base wake. Other devices are added to the sides and the roof of the trailer to generate energized vortices to delay the separation and thereby decrease the base wake. Base plates and Boattail, see Figure 4, demonstrate how base treatment devices can be used at the trailer back in order to reduce the drag from the base region. According to wind-tunnel tests, these devices improve drag by 51 and 44 drag counts, respectively [9].

Figure 4: Base treatment: Base plates and Boattail [9]

2.2 Fluid dynamics

Fluid dynamics is the study of fluids in motion and the physics can be described by three conservation laws [14]:

- Conservation of mass - the continuity equation states that the amount of mass flow that enters a control volume must be equal to the amount leaving it.
- Conservation of Linear momentum (Newton's Second Law of Motion) - given a Newtonian fluid, these equations are used to obtain a relation between pressure, momentum and viscous forces, the equations are called Navier-Stokes equations.
- Conservation of energy (First Law of Thermodynamics) - the energy equation is the law saying that the total amount of energy is conserved within the system, however, it can change between the different states.

Due to the mathematical complexity of the equations it is almost impossible to solve them analytically, except for some simplified cases. However, when working with air at room temperature and a Mach number below 0.3, the fluid can be assumed to have constant density, a so-called incompressible flow. This together with the assumption that the viscosity of the fluid is constant, makes it possible to write the conservation laws as following [14]:

$$\nabla \mathbf{V} = 0 \quad \textit{Continuity equation} \tag{1}$$

$$\rho \frac{\partial \mathbf{V}}{\partial t} = -\nabla p + \mu \nabla^2 \mathbf{V} + \rho \mathbf{g} \quad \textit{Momentum equation} \tag{2}$$

$$\rho c_p \frac{dT}{dt} = k \nabla^2 T + \Phi \quad \textit{Energy equation} \tag{3}$$

where $\mathbf{V} = velocity\ field$, $\rho = density$, $t = time$, $p = pressure$, $\mu = viscosity$, $\mathbf{g} = gravity\ field$ $c_p = specific\ heat\ capacity$, $T = temperature$, $k = coefficient\ of\ thermal\ conductivity$, $\Phi = viscous - dissipation\ function$.

The continuity and momentum equations can be solved independently of the energy equation and when temperature is constant, as assumed in this project, the energy equation is neglected. The continuity and momentum equations describe the motion of the fluid and are solved for velocity and pressure.

Almost all fluid flows are turbulent, that is: stochastic, three-dimensional and time dependent [5]. Due to this chaotic behavior the flow will experience fluctuations, which means that pressure and velocity will be defined as the mean value plus a fluctuation term; $u = \bar{u} + u'$ and $p = \bar{p} + p'$ respectively. To handle this, the equations (continuity and momentum), with additional terms due to fluctuations, are time averaged. The new equations are called Reynolds-Averaged Navier-Stokes equations, abbreviated as RANS [14]:

$$\nabla \bar{\mathbf{V}} = 0 \quad \textit{Continuity equation for the mean flow} \tag{4}$$

$$\rho \frac{\partial \bar{u}}{\partial t} = -\frac{\partial \bar{p}}{\partial x} + \rho g_x + \frac{\partial}{\partial x}\left(\mu \frac{\partial \bar{u}}{\partial x} - \rho \overline{u'^2}\right) + \frac{\partial}{\partial y}\left(\mu \frac{\partial \bar{u}}{\partial y} - \rho \overline{u'v'}\right) + \frac{\partial}{\partial z}\left(\mu \frac{\partial \bar{u}}{\partial z} - \rho \overline{u'w'}\right)$$
$$\textit{Momentum equation in } x - \textit{direction}$$

$$\rho\frac{\partial\bar{v}}{\partial t} = -\frac{\partial\bar{p}}{\partial y} + \rho g_y + \frac{\partial}{\partial x}\left(\mu\frac{\partial\bar{v}}{\partial x} - \rho\overline{u'v'}\right) + \frac{\partial}{\partial y}\left(\mu\frac{\partial\bar{v}}{\partial y} - \rho\overline{v'^2}\right) + \frac{\partial}{\partial z}\left(\mu\frac{\partial\bar{v}}{\partial z} - \rho\overline{v'w'}\right)$$

$$Momentum\ equation\ in\ y - direction$$

$$\rho\frac{\partial\bar{w}}{\partial t} = -\frac{\partial\bar{p}}{\partial z} + \rho g_z + \frac{\partial}{\partial x}\left(\mu\frac{\partial\bar{w}}{\partial x} - \rho\overline{u'w'}\right) + \frac{\partial}{\partial y}\left(\mu\frac{\partial\bar{w}}{\partial y} - \rho\overline{v'w'}\right) + \frac{\partial}{\partial z}\left(\mu\frac{\partial\bar{w}}{\partial z} - \rho\overline{w'^2}\right)$$

$$Momentum\ equation\ in\ z - direction$$

2.3 Computational Fluid Dynamics (CFD)

Computational Fluid Dynamics, usually and from here on abbreviated to CFD, is a numerical method to compute the dynamics of a fluid. In brief, it is implemented by dividing a computational domain into small cells where the flow is modeled and flow equations are solved. Since almost all fluid flows are turbulent, different CFD methods are used in order to simulate turbulence. These can be divided in different categories where some of them are; Turbulence models for Reynolds-Averaged Navier-Stokes (RANS) equations, Large Eddy Simulation (LES), Direct Numerical Simulation (DNS) and Lattice Boltzmann method (LBM). The LBM differs from the other methods by simulating the movements of particles and aims at recover the hydrodynamics of the Navier-Stokes equation. RANS on the other hand, uses the Navier Stokes equations as a starting point and aims at solving them [10]. DNS does not use a turbulence model; it computes all the turbulent velocity fluctuations and therefore demands both small time steps and cells that require substantial computer resources. LES focus on the large eddies in the flow and requires quite large computer resources. However, the most common way to simulate turbulence is to calculate the time-averaged properties of the flow, such as mean pressure, mean velocity and so on, which in most cases give sufficient information about the flow. This method has a modest computer demand and is conducted with RANS-models [13].

2.3.1 Turbulence models for Reynolds-Averaged Navier-Stokes equations

There are several different turbulence models within the RANS method that in different ways models the extra terms that forms when the Navier-Stokes equations are time-averaged. Some models worth mentioning are Mixing length model, $k-\varepsilon$ model, $k-\omega$ model and Reynolds stress model, which have none, two, two and seven additional transport equations respectively, which needs to be solved in addition to the RANS equations [13]. Naturally, all models have their advantages and disadvantages; the Mixing length model is not suitable for flows with separation and circulations, and the Reynolds stress model is the most complex one of these four and needs fairly large computer capability. Left are the two two-equation models $k-\varepsilon$ and $k-\omega$.

Both $k-\varepsilon$ and $k-\omega$ are so-called Eddy viscosity models, which means that they are based on turbulent viscosity. In the $k-\varepsilon$ model the two transports equation are solved for the turbulent kinetic energy k and its dissipation ε. ω is the dissipation rate per unit turbulence kinetic energy, in other word the specific dissipation rate $\omega \backsim \varepsilon/k$. One of the major differences between these two models is that the standard $k-\varepsilon$ model needs wall functions to resolve the boundary layer, whereas the $k-\omega$ model is feasible to use all the way into the wall [3]. The $k-\omega$ model on the other hand, deals with problems when it comes to the initial value of ω in the free stream, the results seems to depend on this value.

In order to obtain the best features of the two models, Menter developed a modified $k - \omega$ model 1992 called Shear Stress Transport (SST) $k - \omega$ turbulence model. This model is a mix between $k - \varepsilon$ and $k - \omega$, and uses the near-wall features from the $k - \omega$ model close to the wall and then applies the $k - \varepsilon$ model in the free-stream regions away from the wall. SST $k - \varepsilon$ turbulence model is chosen for this project since it is widely used in vehicle aerodynamics and is efficient and accurate [12].

2.3.2 Computational domain

The computational domain and its cells, the so-called volume mesh, can be generated and designed in different ways. The cells can be constructed in shapes of tetrahedra, hexahedra and polyhedra. The different cell types have different advantages and disadvantages that depend on the geometry and flow characteristics. For this project the hexahedral mesh with prism layers has been chosen since it is faster to generate and requires less memory, compared to the polyhedral mesh for example. For external aerodynamic flow simulations that have a predominately streamlined flow, the hexahedral mesh also gives a faster convegence. These are the reasons why this mesh type is recommended by CD-adapco, the distributor of STARCCM+, for these types of simulations.

The mesh is generated with the Octree method. This method divides the computational domain into small cubes, which are subdivided until they reach a desired resolution. Each subdivision dimidiates the size of the cube and provides a smooth variation in cell size [4].

3 Methodology

In this chapter the procedure of this project is described. As mentioned in Chapter 1, this project is conducted by evaluating different drag reducing trailer devices by means of CFD. ANSA and STARCCM+ are the software used and the setup and essential settings are described in Subchapter 3.1. Information about the selected devices is presented in Subchapter 3.2. Further on, from the evaluation of the individual devices, combinations of these are tested and analyzed to see if drag can be improved even more.

In all cases the trailer is pulled by a Volvo FH-H2 tractor, see Figure 5, which is used for long-distance transports of heavy goods. The tractor used in this project includes aerodynamic truck devices such as roof deflector, side deflectors and chassis fairings.

Figure 5: Volvo FH-H2 tractor

3.1 Case Setup

To obtain comparable results, all chosen cases are generated from the same reference model with the same procedure and settings.

3.1.1 Geometry

CAD-models of the tractor and a simplified box trailer are given by Volvo and are imported into ANSA. Small adjustments are done on the trailer to obtain correct dimensions. Trailer devices are created as CAD-models in ANSA. To be able to set different boundary conditions and mesh values on certain parts, the geometries are divided and given a Property ID (PID) in ANSA. This gives the possibility, for example, to set rotating wheels, specify a specific mesh setting or to study the drag contribution on a certain part. The CAD-models are then exported to STARCCM+ as a surface mesh.

3.1.2 Volume mesh

From the surface mesh imported from ANSA, a closed, manifold and non-intersecting surface is created in STARCCM+ by using the *Surface wrapper* feature. This wrapped surface is then further improved by the *Surface remesher* feature, which creates a high quality triangulated surface mesh. The *Trimmer meshing* *model* then uses the Octree technique to produce a dominant hexahedral volume mesh in the wind tunnel. In addition to these meshing models a *Prism layer meshing model* is used to obtain the prism layers closest to the surface. These thin layers of cells are needed in order to resolve the inner part of the boundary layer and thereby handle the high velocity gradients here.

In regions of predictable flow separation and where unsteady wakes are created, like the base wake of the trailer, a large number of small cells are used in order to improve the resolution and the robustness of the overall solution. Due to time limitation, the volume mesh around the truck is arranged to $40 - 43$ million cells. Pictures of the refinement boxes with different cell size and a representation of the prism layers are seen in Figure 6. Further detailed information about the mesh settings is found in Appendix A.

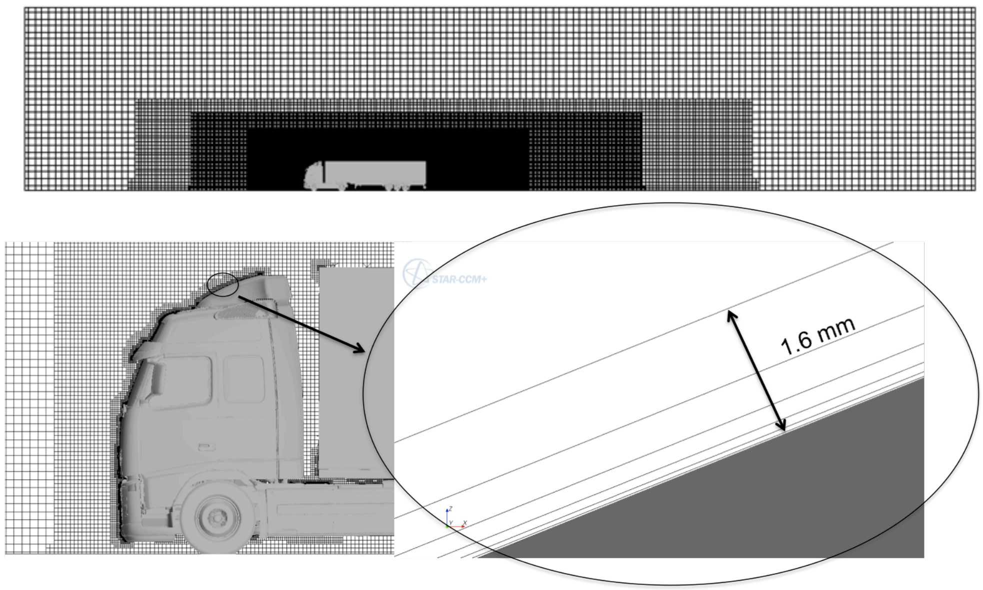

Figure 6: Volume mesh of the computational domain with zoom of the prism layers

3.1.3 Physical models

Below follows a brief description and clarification of the most essential models used for the simulations in STARCCM+. Solver settings are found in Appendix B.

- **Space** - *Three dimensional*
- **Motion** - *Stationary*
- **Time** - *Steady*
- **Material** - *Gas* - Air
- **Flow** - *Segregated Flow* solves the pressure and velocity equations in an uncoupled way
- **Equation of state** - *Constant Density*
- V**iscous Regime** - *Turbulent*
  - **Turbulence model** - *Reynolds Averaged Navier Stokes - SST Menter $k - \omega$ turbulence model*

  * $k-\omega$ **wall treatment** - *All y+ Wall Treatment* is the recommended wall treatment for the $k-\omega$ model since it enables wall functions for coarser grid where $y^+ > 30$ and a low-y^+ wall treatment, assuming well resolved sublayer and omitting the wall functions, where $y^+ \to 0$ [3].

- *Cell Quality Remedation* is used to obtain solutions on a poor-quality mesh. The model searches for poor-quality cells and their neighbors (depending on user defined criteria) and then computes the gradients in these cells. The gradients are then modified in a way to improve the robustness of the solution [3].

In order to model the cooling package in the front of the tractor, which constitutes a great flow resistance for the air when it goes through it, a porous medium is used. The Condensor, the Charge air cooler and the Radiator are all simulated with porous mediums of different inertial and viscous resistance to obtain the accurate pressure drop that occurs in reality.

3.1.4 Boundary conditions

During realistic circumstances and driving conditions, the truck is subjected to cross-winds from several different directions. To obtain a drag value that corresponds to the average of the different cross-winds, a weighted value from several different yaw angles is calculated during wind-tunnel tests conducted by Volvo. However, during CFD-simulations, only two yaw angles are used to save time. The weighted value is calculated from 0° and 5° yaw simulations, according to Equation 6 in Subchapter 3.3. This formula is used in-house at Volvo and corresponds to the weighted value used in wind-tunnel tests.

To simulate two yaw conditions the wind tunnel is divided into several parts; ground, inlet, outlet, side walls and roof. In 0° yaw the inlet is set to *velocity inlet*, whereas the side walls are defined as *stationary wall* with slip condition to simulate symmetry. The slip condition makes sure that there no shear stress disturbs the flow and that the velocity gradient is zero across the boundary. This boundary condition also applies to the roof of the tunnel. To simulate cross-wind condition the boundary condition at the side walls is set as *velocity inlet* since the airflow hits the wind tunnel with a 5° yaw angle. The cross-wind velocity, $v_{cross-wind}$, is then calculated from the knowledge of the velocity in x-direction (v_x) and the yaw angle of the cross-wind. Figure 7 demonstrates how the cross-wind is simulated in the wind tunnel in STARCCM+. To save time, the same mesh used in 0° yaw is used for 5° yaw.

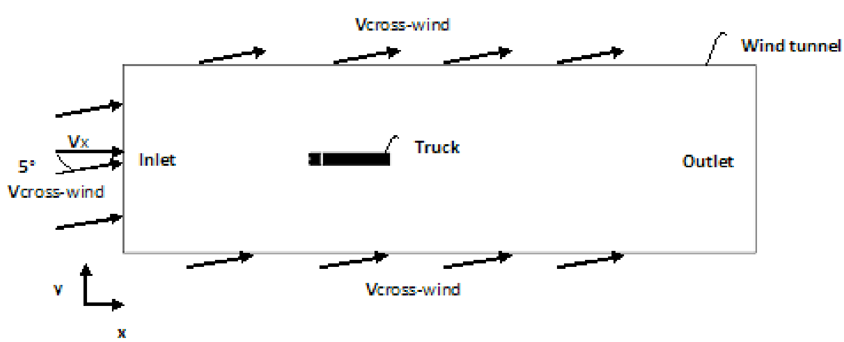

Figure 7: Simulation of cross-wind

To simulate the rigid parts such as the tractor and the trailer, stationary wall with no slip condition is used as boundary condition. Moving ground and rotating wheels, together with velocity inlet and pressure outlet, are used to simulate the movement of the truck. Further information about the boundary conditions is found in Table 1.

Table 1: Boundary conditions

Tractor	Stationary wall - no slip	
Tractor wheels	Moving wall - no slip Local rotation rate	443.5205 rpm
Trailer	Stationary wall - no slip	
Trailer wheels	Moving wall - no slip Local rotation rate	437.9329 rpm
Tunnel ground	Moving wall in x-direction	25 m/s
Tunnel inlet	0º yaw: Velocity inlet	25 m/s
	5º yaw: Velocity inlet ($v_{cross-wind}$ components: x=0.9962, y=0.0872)	25.0955 m/s
	Turbulence intensity	0.0050
	Turbulent viscosity ratio	1
Tunnel outlet	Pressure outlet	0 Pa
	Turbulence intensity	0.0050
	Turbulent viscosity ratio	1
	Backflow direction specification	Boundary Normal
Tunnel side walls	0° yaw: Stationary wall - slip	
	5º yaw: Velocity inlet ($v_{cross-wind}$ components: x=0.9962, y=0.0872)	25.0955 m/s
Tunnel roof	Stationary wall - slip	

3.1.5 Simulation

The simulations are performed in STARCCM+ and each simulation runs for 5000 iterations. To make sure that the solution is stabilized, the convergence is checked from the residuals and the drag-plot. The drags from the two yaw cases are acquired by calculating the mean value of the last 500 iterations.

3.2 Case Definitions

The selected cases are presented in Table 2 and an additional description of each case is given further down in this section. The devices are generated from information obtained through a research of today's market, although without drawings. The design of the devices is therefore a combination of existing products and own designs by the authors, constructed in consultation with supervisor at Volvo. Dimensions of the trailer and the devices can be found in Appendix C.

Table 2: Selected cases

	Reference
Gap treatment	Sealed gap
	Vortex stabilizer
	Gap fairing
Base treatment	Side plates
	Base plates
	Frame extension
Undercarriage treatment	Side skirts
	Sealed wheels
	Smooth underbody
Aerodynamic trailer designs	Teardrop
	Basedrop

Reference The *Reference* case represents an unmodified box trailer including side bumpers and a spare wheel placed underneath the fore part of the trailer, see Figure 8. All three wheel pairs are in contact with ground and set to rotate.

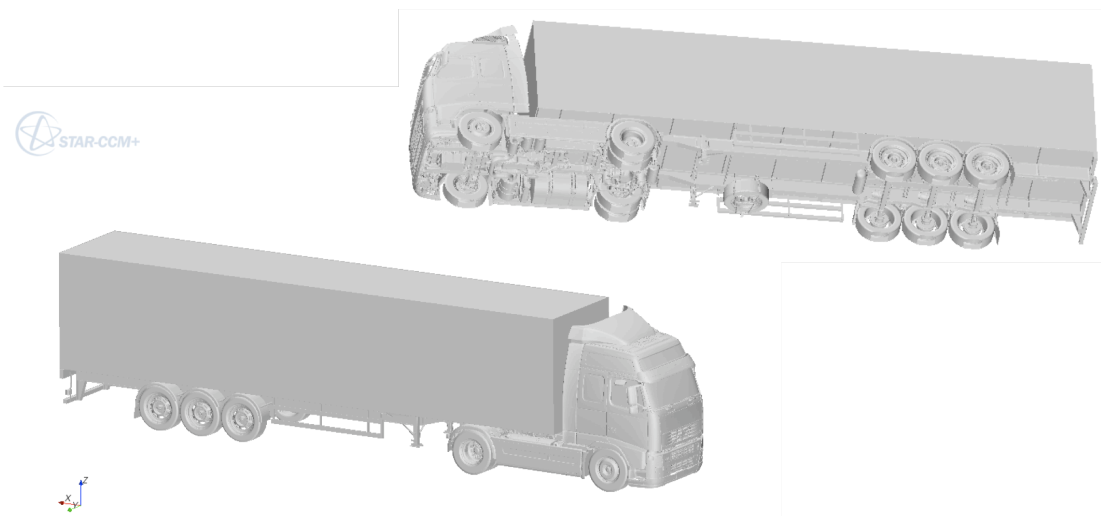

Figure 8: The Reference

Gap treatment The selected gap treatment devices are shown in Figure 9. *Sealed gap* symbolizes the ideal case when it comes to tractor-trailer gap treatment and is seen Figure 9a. The whole gap is sealed to avoid flow disturbing cross-winds. So far this device is not a realistic solution since no consideration is taken to the truck's turning ability. Although, it is still interesting to test this solution to see the gap clearance's contribution to drag.

Vortex stabilizer consists of two equal plates applied at the trailer front. The main objectives of the *Vortex stabilizer* are to reduce the disturbances from the cross-winds and to create stable vortices in the gap. *Gap fairing* is used to improve the re-attachment of the flow on the trailer roof and to reduce the pressure peaks at the upper corners and at the edges of the trailer front. It is also designed to reduce the side clearance between the tractor and the trailer.

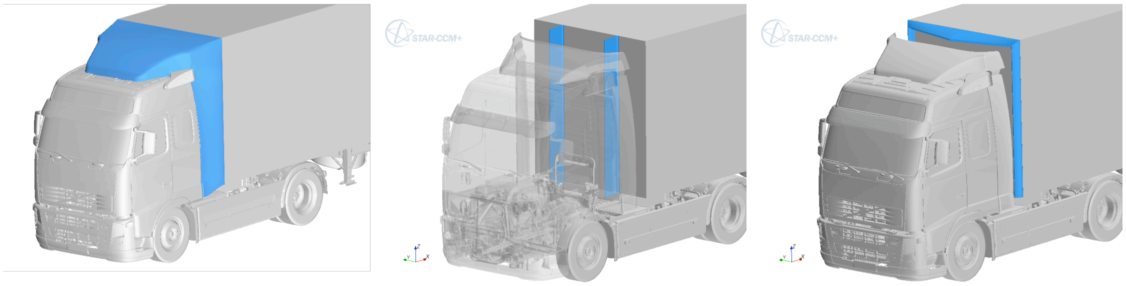

(a) Sealed gap (b) Vortex stabilizer (c) Gap fairing

Figure 9: Devices to improve the flow in and around the gap

Base treatment Figure 10 represents the selected base treatment devices. *Side plates* are applied at the trailing edges on the sides of the trailer, whereas *Base plates* are placed at the bottom and top of the trailer, see Figure 10a and 10b. The aim of adding these plates is to improve the drag by reducing the base wake. According to previous research [1], optimal functionality of such plates is achieved with an inward angle of 13° and a plate width that is $1/4$ of the trailer width. This is applied to both *Side plates* and *Base plates*. *Frame extension* is a combination of *Side plates* and *Base plates*, see Figure 10c.

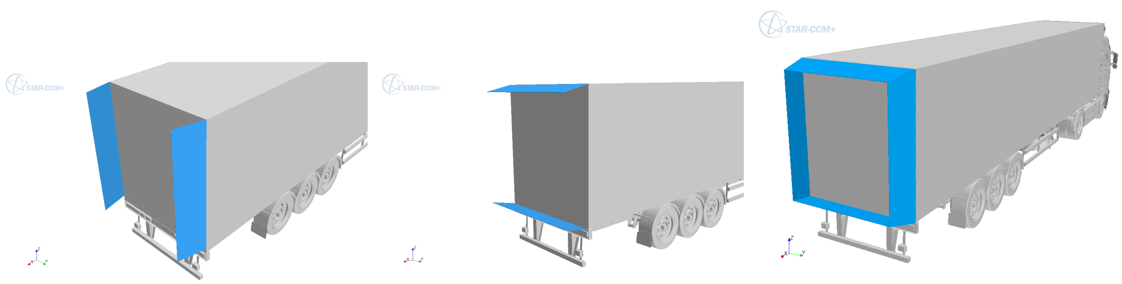

(a) Side plates (b) Base plates (c) Frame extension

Figure 10: Base treatment

Undercarriage treatment The undercarriage devices are represented by *Side skirts*, *Sealed wheels* and *Smooth underbody*, see Figure 11. The advantage of *Side skirts* is the improvement of the flow along the sides of the trailer at ground level. Furthermore, a side-diffuser is implemented at the rear of the *Side skirts* for improvements of the flow at the rear. To see the effect from the rotating trailer wheels, *Side skirts*is also modified with covered wheels and the case is called *Sealed wheels.*

Smooth underbody represents a trailer where all the irregular geometries and beams are covered with a smooth surface, see Figure 11c. This configuration might not be a realistic solution, it is nevertheless tested to obtain an understanding of how the undercarriage affects the airflow underneath the trailer and in the base wake.

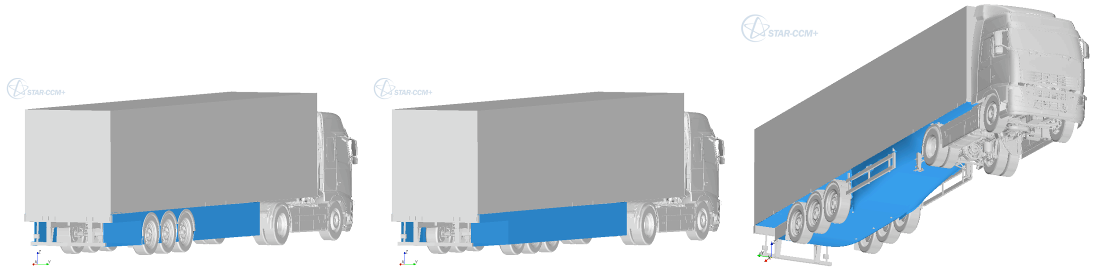

(a) Side skirts (b) Sealed wheels (c) Smooth underbody

Figure 11: Side skirts, Sealed wheels and Smooth underbody

Aerodynamic trailer designs *Teardrop* is a modification of the trailer shape. Its roof is designed to improve the flow over the truck and to reduce the base wake. Due to restrictions, such as maximum height and that it is decided not to do any adjustments of the tractor in this project, the shape of the teardrop is limited. The height of the trailer used in this project is 4 meters and due to the Swedish height legislations of 4.5 meters, 0.5 meters of added material is being used to shape the trailer. This means that nothing is removed from the trailer's loading volume. The trailer is seen in Figure 12.

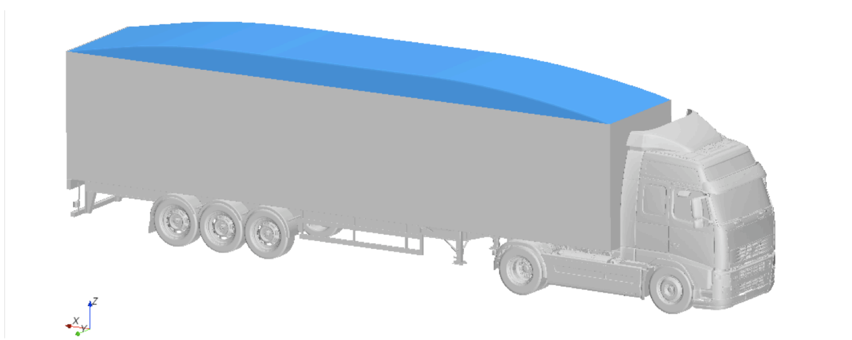

Figure 12: Teardrop

Basedrop is a configuration of the trailer geometry that is constructed to evaluate how much the drag can be reduced if sacrificing the area of one pallet. By removing one pallet in the last row, it is possible to decrease the width of the trailer in the rear and shape it in an aerodynamic beneficial way. The configuration is named *Basedrop* and is seen in Figure 13.

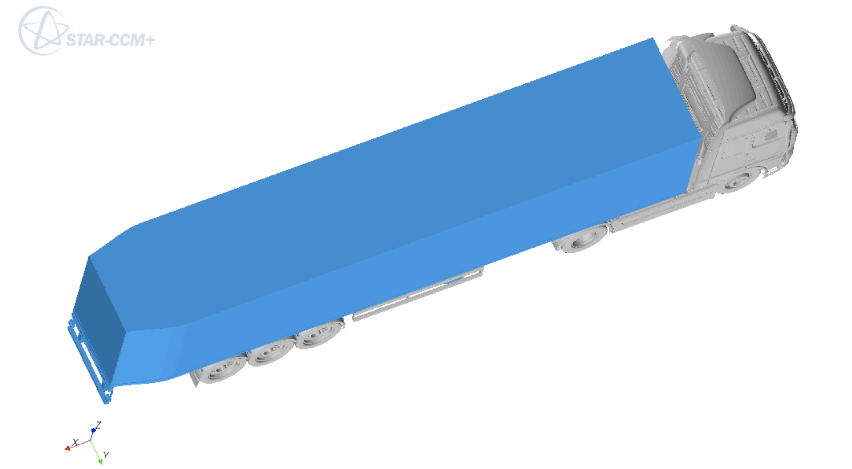

Figure 13: Basedrop

3.3 Aerodynamic drag calculations

The drag coefficient (C_d) is useful when comparing the aerodynamic efficiency between different vehicles. It is related to the aerodynamic drag force (F_d), vehicle speed (V), frontal area (A) and the density (ρ), see Equation 5.

$$C_d = \frac{F_d}{\frac{1}{2} \cdot \rho \cdot A \cdot V^2} \tag{5}$$

As mentioned in Subchapter 3.1, the truck is simulated in 0° and 5° yaw. The weighted value of these two is calculated by Equation 6 and results in a cross-wind angle of approximately 3.1°.

$$C_{d-weighted} = {}^1\!/_3 \cdot C_{d-0deg} + {}^2\!/_3 \cdot C_{d-5deg} \tag{6}$$

To simplify comparison of the cases, the drag is usually presented as the difference in drag counts (DC) between the specific case and the reference case. Drag counts is calculated according to Equation 7.

$$DC = \Delta C_d \cdot 1000 \tag{7}$$

$$where \quad \Delta C_d = C_{d-specific\ case} - C_{d-reference}$$

To obtain an understanding of how a reduction of drag affects the fuel consumption, the drag improvement can be recalculated into fuel saving in percent (FS), see Equation 8.

$$FS\ (\%) = \frac{\Delta C_d \cdot 16}{30} \tag{8}$$

The factor of 16 in the fuel saving formula is based on experiments of a long-distance transport with a truck of 40 ton. The denominator of 30 is based on an assumed fuel consumption of $30L/100km$. This fuel saving evaluation is the formula used in-house at Volvo and the result should be considered with care since several factors influence the fuel consumption.

4 Results and Analysis

This chapter presents the results from the simulations and is divided into four parts. First a detailed analysis of the reference case is done to identify problematic flow regions and to obtain an understanding of the flow behavior. Then the result of the individual devices are showed and compared with the reference case, followed by an evaluation of how the devices can be combined to improve the results. The results of these combinations are then presented and analyzed in the last part.

4.1 Reference

As seen in Figure 14, representing iso surfaces of total pressure equal to zero, large wake structures appears around the truck. These unsteady wake structures symbolize large energy losses in the flow which contributes to drag. In 0° yaw, there is an almost symmetric wake created around the truck. Large wake structures are especially observed along the sides of the truck, origin from the separation at the front and amplified by rotating wheels and the disturbed flow underneath the truck. The flow losses along the trailer are then reduced until it reaches the rear part of the trailer where the air again separates and a large base wake is created.

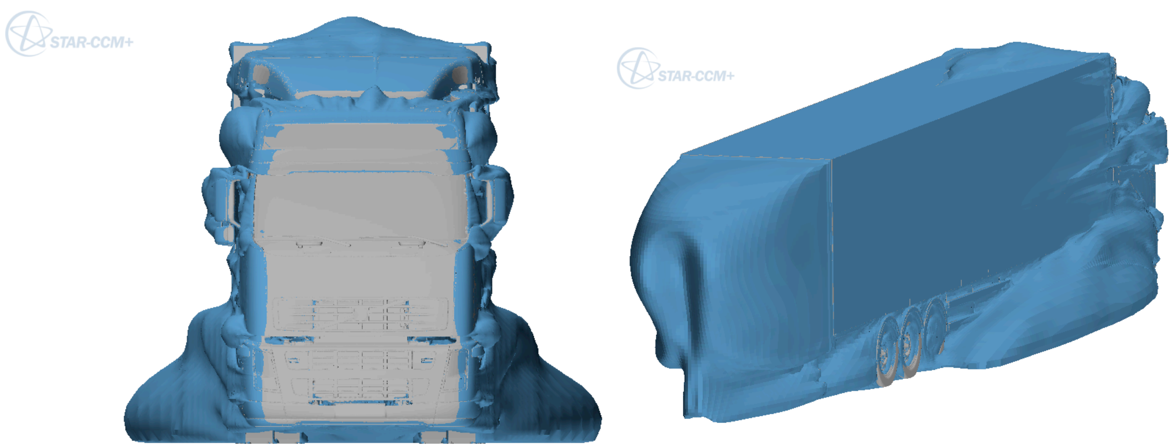

Figure 14: The reference case, iso surfaces of total pressure equal to zero in 0° yaw

In 5° yaw, see Figure 15, the flow losses dominates at the leeward side of the truck and an asymmetric wake structure is created. The large wake at the leeward side is a result of the increased airflow through the gap and the undercarriage. In 5° yaw the drag is increased with approximately 180 DC.

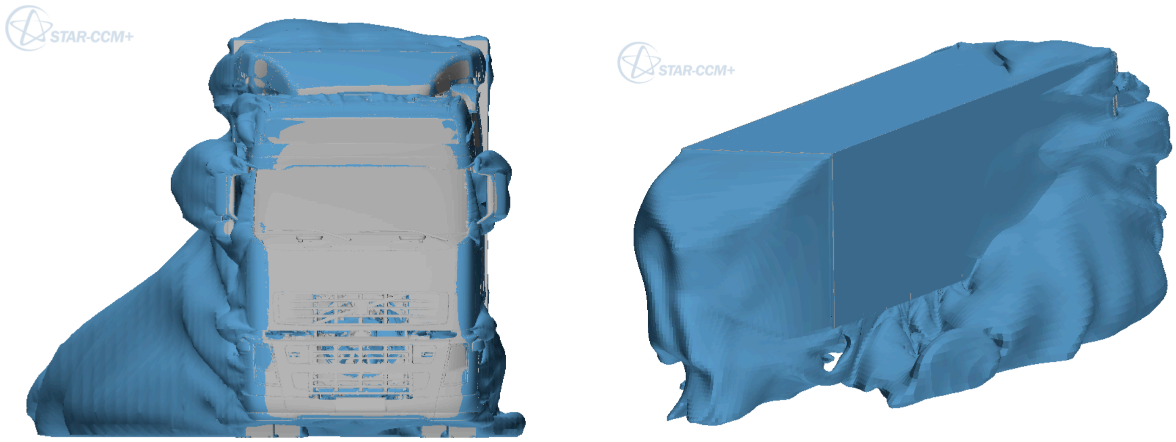

Figure 15: The reference case, iso surfaces of total pressure equal to zero in 5° yaw

In Figure 14, a small wake can be observed just above the mirror, created from the air passing over the sun visor. Together with the air that interacts with the engine air-intake, placed on the left side, these two flow phenomena contributes to a vortex that continues along the left edge of the trailer roof, see Figure 16.

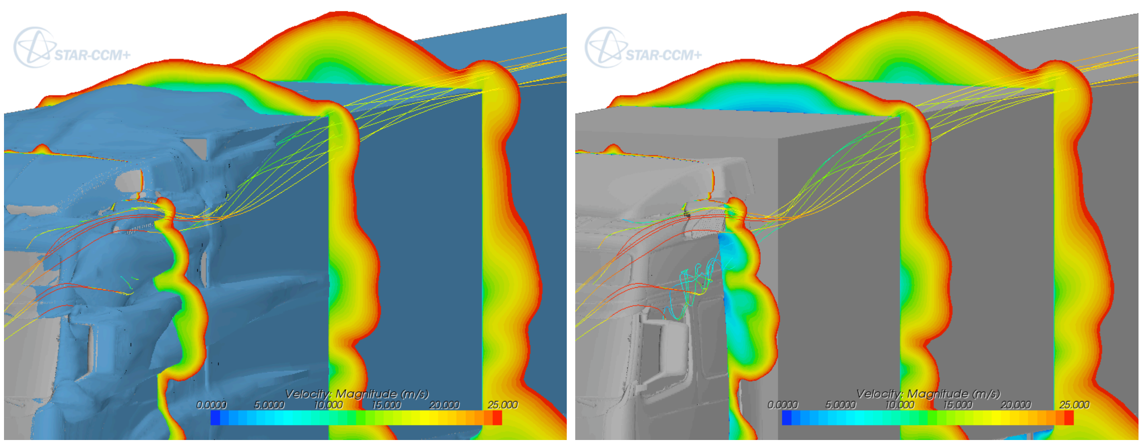

Figure 16: Streamlines and velocity magnitude illustrating the formation of the flow structure along the trailer roof, with and without iso surface

Figure 17 visualizes the velocity development along the trailer. It is seen that the velocity profile corresponds to the iso surfaces in Figure 14 and 15, indicating that the wakes contain low velocities due to separation. A low-momentum flow deteriorates the attachment of the air and this can for example be seen along the sides and the roof of the trailer.

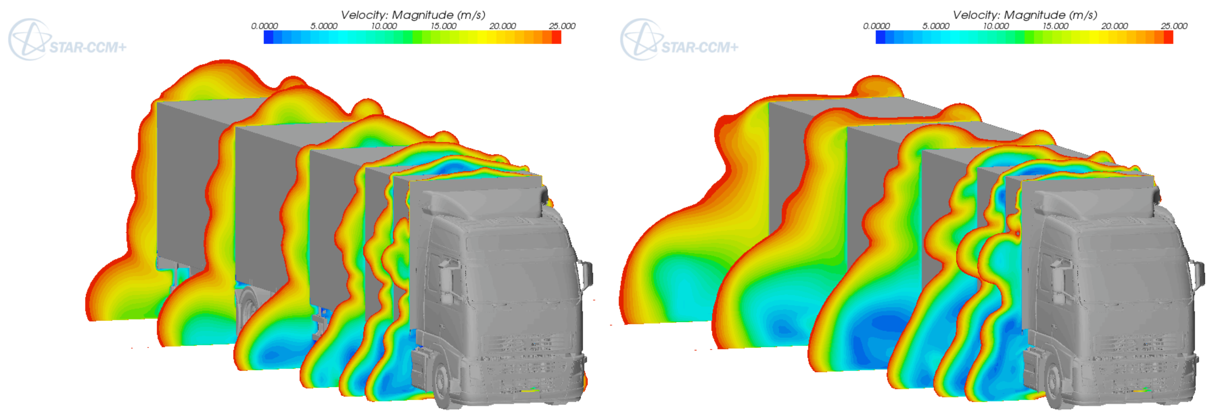

(a) 0° yaw (b) 5° yaw

Figure 17: Velocitiy magnitude displayed in x-planes along the trailer

Even though there are significant differences between the two yaw conditions, the major energy losses still origin from the three critical regions mentioned in the theory; the gap clearance between the tractor and the trailer, the undercarriage and at the rear of the trailer. Obviously these regions are of great interest and are analyzed further in following subchapters.

Tractor-trailer gap

Figure 18 shows the pressure coefficient, the pressure normalized with the velocity, on the trailer front. In 0° yaw, large pressure peaks are observed at the upper corners and at the upper side edges of the trailer front. These high-pressure regions occur as air separates at the trailing edge of the tractor's roof- and side deflector and hits the trailer. This gives an indication of areas at the trailer front where the roof- and side deflectors work poorly. In 5° yaw these regions are relocated and accumulated at the left side of the trailer front where the wind is coming in.

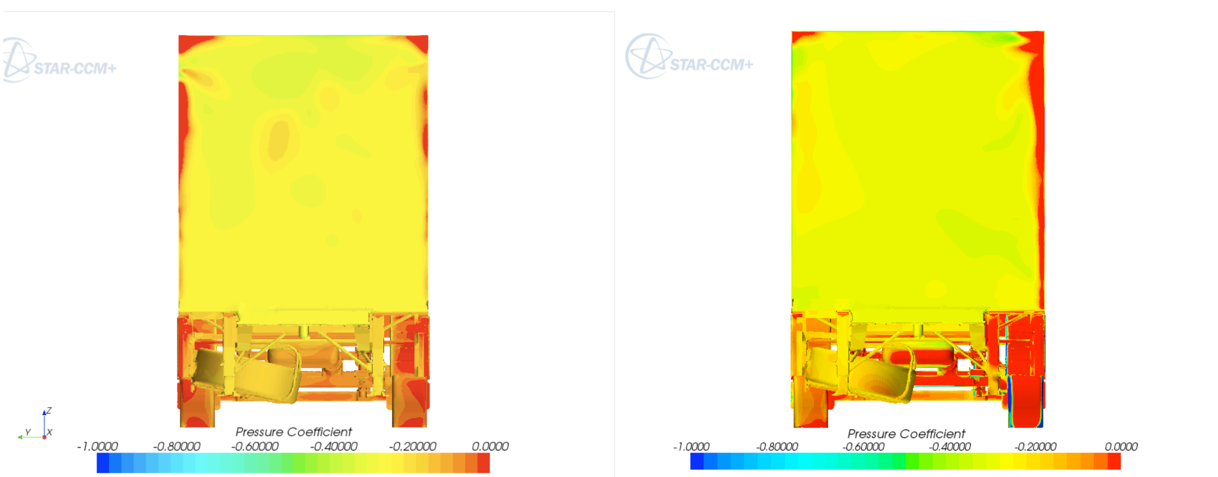

Figure 18: Pressure coefficient on the trailer front for 0° yaw and 5° yaw, respectively

Figure 19a shows the pressure coefficient in the symmetry plane in 0° yaw. Three low-pressure bubbles are observed; two at the roof of the tractor and one at the fore part of the trailer roof. The low-pressure bubbles on the cab are an effect of flow acceleration over the rounded edges, as the flow stays attached to the surface. The low-pressure bubble at the trailer roof is caused by the wake that is created when the flow separates at the trailing edge of the tractor's roof-deflector. The wake itself contains low pressure and low velocities, see Figure 19b, and forces the air to go around it. This causes an acceleration of the around-going flow and hence an expansion of the low-pressure region.

Evaluation of where the air enters and exit the gap clearance in 0° yaw, by means of streamlines and mass flow calculations, shows that the air goes into the gap from the engine compartment and through the side clearance. Even though there is a fairly large gap at the top, not much air enters the gap here due to the angle of the tractor roof deflector that directs air over the gap. Instead, the top of the gap is where most of the air exits and probably contributes to the separation bubble at the fore part of the trailer roof. Some of the air also leaves the gap through the side clearance.

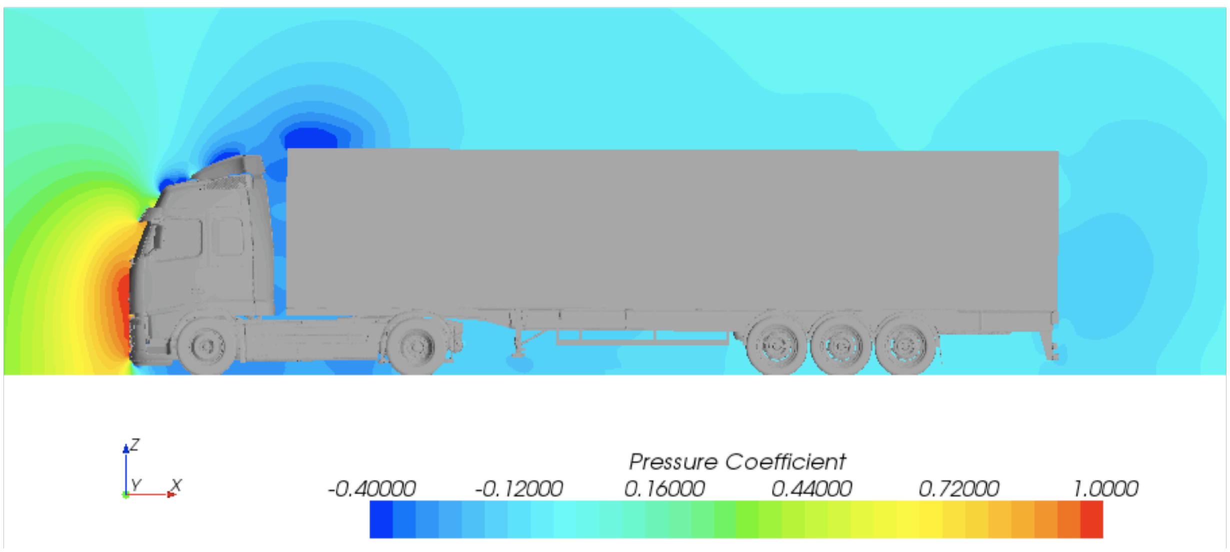

(a) Pressure coefficient displayed in the symmetry plane

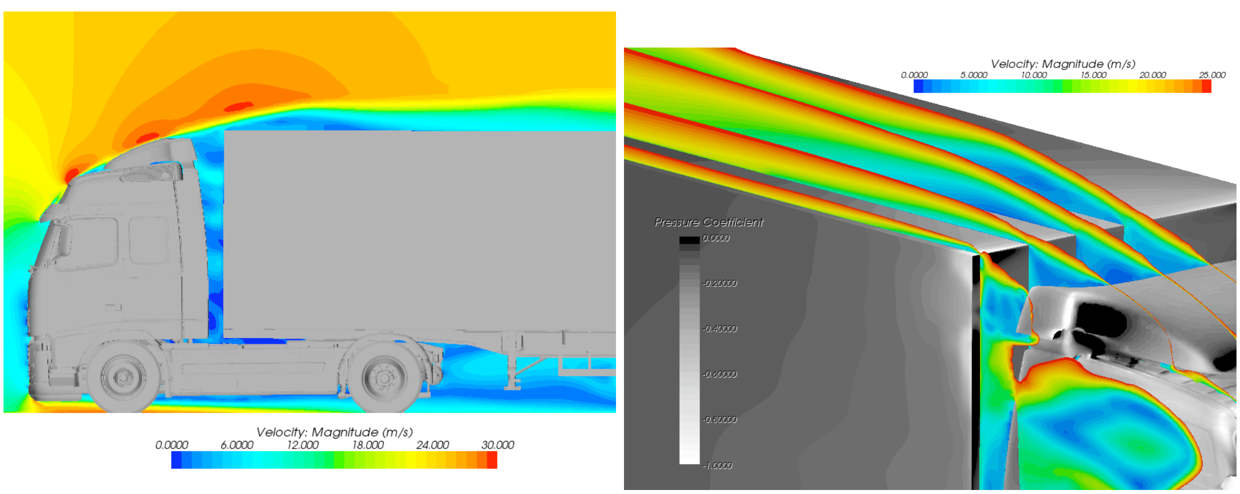

(b) Velocity magnitude in the symmetry plane and in different y-planes

Figure 19: The reference case in 0° yaw

By displaying velocity vectors in x and z-plane for 0° yaw, Figure 20a, it is obvious that the flow in the gap contains a lot of swirls and is very irregular. The same applies for cross-wind condition, although with a larger amount of air that travels from the windward side to the leeward side. This results in a significant flow separation on the leeward side of the truck, see Figure 20b.

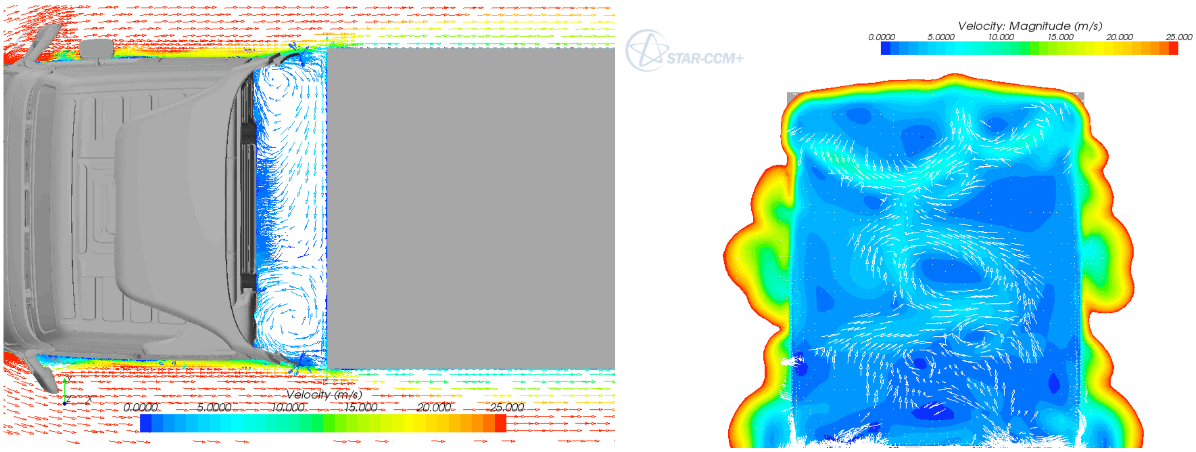

(a) 0° yaw

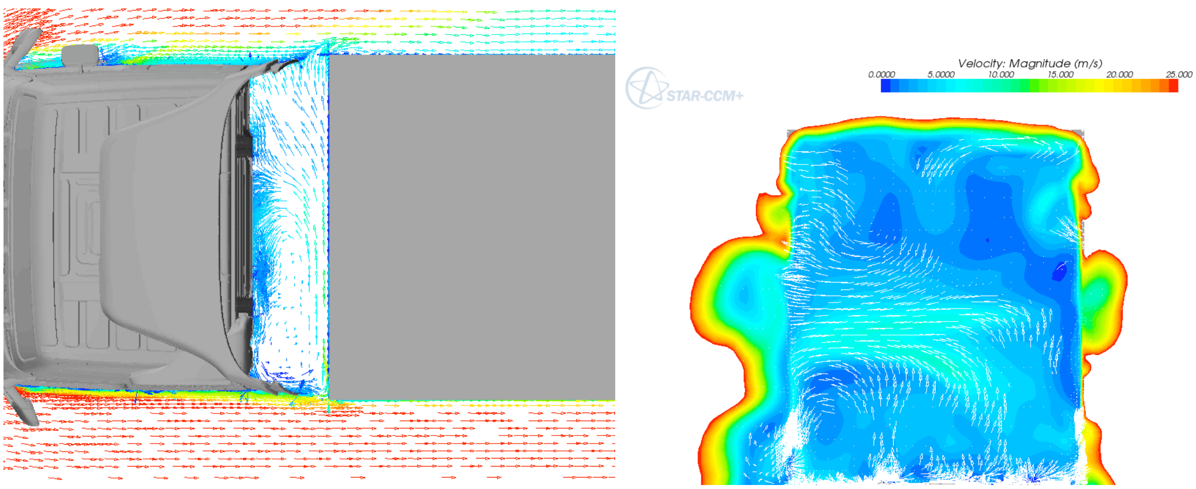

(b) 5° yaw

Figure 20: Velocity illustrations of the gap flow. To the left: velocity vectors displayed approximately 1900mm above the ground. To the right: the velocity magnitude and vectors displayed 200mm in front of the trailer.

Undercarriage

Pictures of the airflow underneath the trailer indicates a very disturbed and chaotic behavior. The air that reaches the undercarriage of the trailer is already separated and turbulent due to flow disturbances from the tractor and its rotating wheels. Pictures from the 0° yaw simulations reveals low velocities under the trailer and many large swirls at the fore part of the trailer undercarriage. In Figure 21, streamlines are released from the plane in the exit zone at the rear part of the undercarriage, indicating that almost all the air that exits here enters at the posterior part of the undercarriage. A very small amount of air seems to travel throughout the whole undercarriage region.

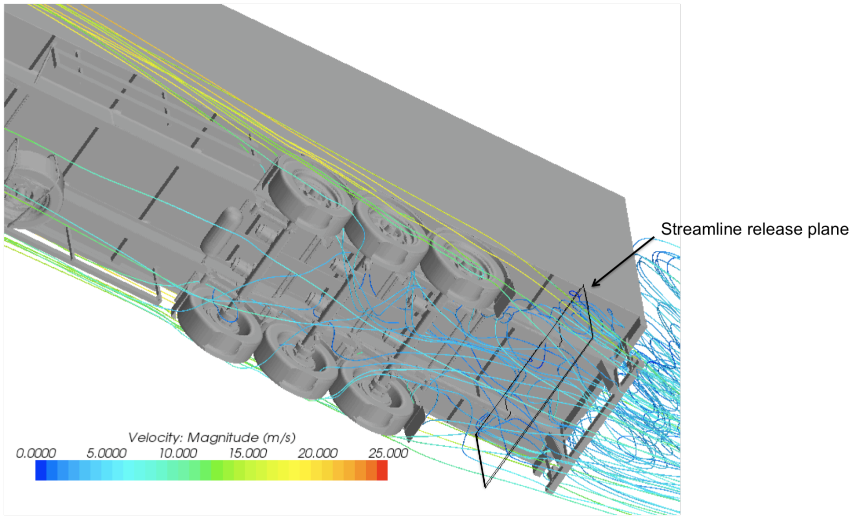

Figure 21: Streamlines released from a plane at the rear of the undercarriage, 0° yaw.

In 5° yaw, the flow disturbances under the trailer are increased. In contrast to 0° yaw, a large amount of cross-winds with high velocity enters the undercarriage. The velocity of the flow is then significantly reduced as it hits the wheel bogies and the wheels. This creates a low-momentum flow underneath the trailer that separates at the rear. Furthermore, an extended wake structure with low velocity is created at ground level on the leeward side of the trailer.

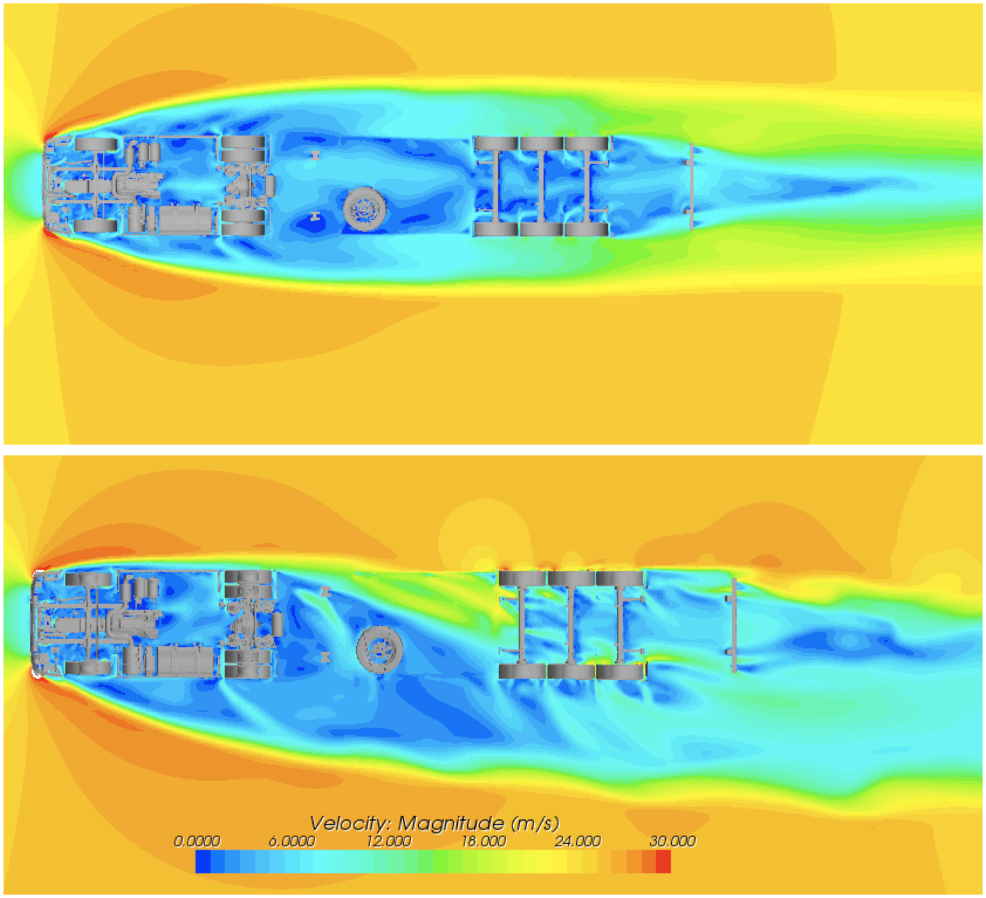

Figure 22: Velocity magnitude displayed 500 mm above ground in 0° and 5° yaw, respectively.

Rear of the trailer

Just behind the trailer a large wake is generated as air separates from the surface at the trailing edge at the rear of the trailer. A low-pressure region is created behind the trailer when the separation occurs and air is sucked into the wake from all the sides. The low-momentum flow that exits from the undercarriage turns upward straight after the trailer and generates an upwash and a swirl behind the trailer. In the center of a swirl a substantial low pressure is obtained. At the upper part of the base wake, larger swirls are created due to the higher velocity of the air that travels over the roof. This is seen in Figure 23a that visualizes the airflow behind the trailer. The same figure also shows, during cross-wind condition, how the low pressure on the trailer back decreases even more and contributes to the increased drag.

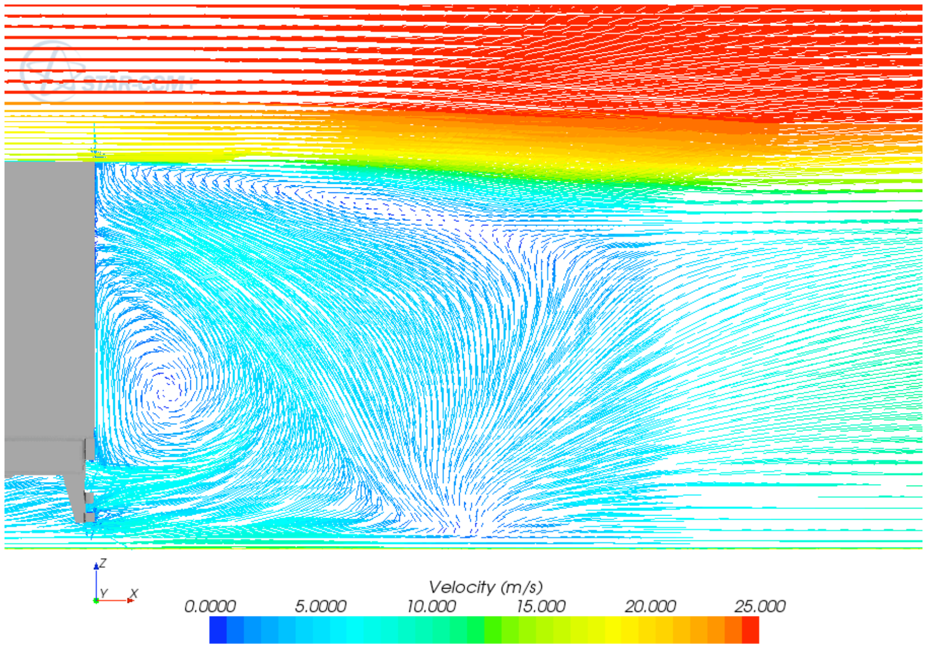

(a) Velocity vectors displayed in symmetry plane, 0° yaw

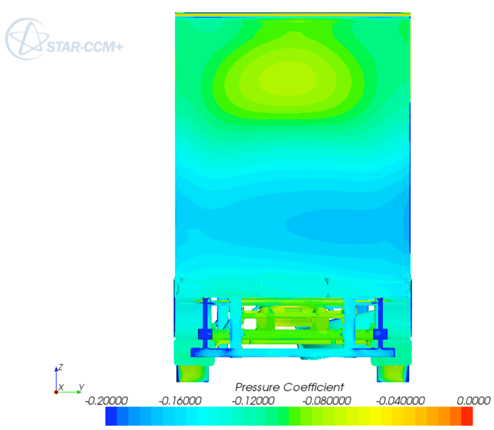

(b) Pressure coefficient on trailer back, 0° yaw

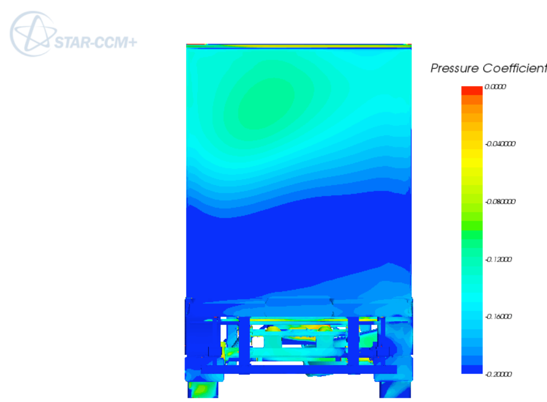

(c) Pressure coefficient on trailer back, 5° yaw

Figure 23: Velocity vectors and pressure in the base wake

4.2 Results of individual devices

Figure 24 shows the results from the simulations of the individual devices. Further down a more detailed review is presented for each device.

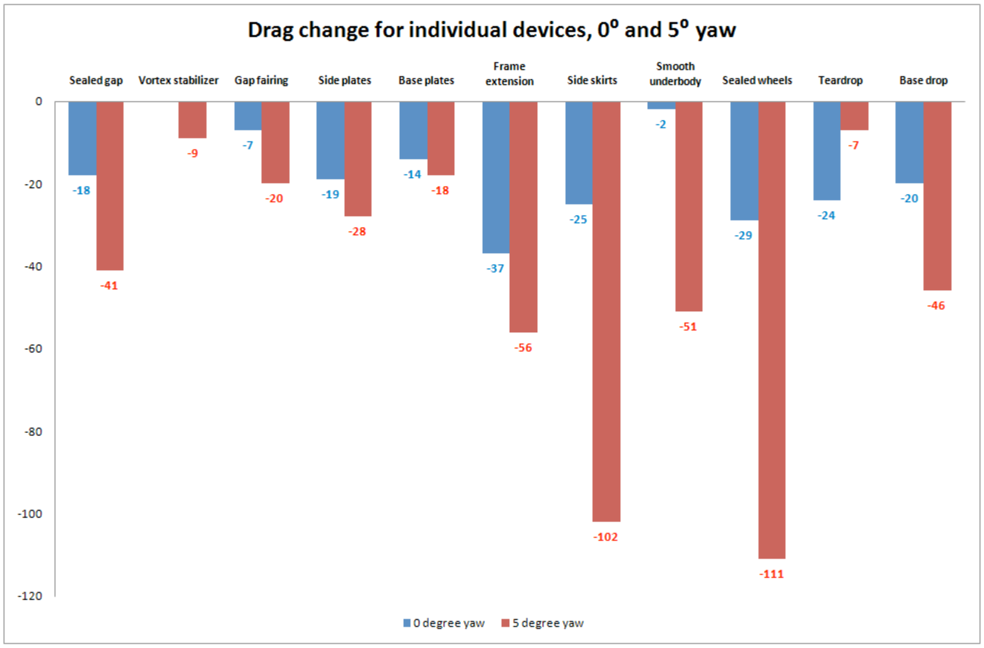

Figure 24: The results of the individual devices in 0° and 5° yaw.

4.2.1 Sealed gap

Pictures of the flow around *Sealed gap* shows that the air follows the gap sealing very well and that the boundary layer along the trailer roof is reduced. Table 3 confirms the improvements with a drag reduction of 33 drag counts for the weighted C_d value.

Table 3: Change in drag when closing the gap

DC - 0° yaw	DC - 5° yaw	Weighted DC
-18	-41	-33

As seen in Figure 25, *Sealed gap* shows a very good flow attachment over the gap and along the trailer roof in 0° yaw, compared to the *Reference*. The pictures also show that the velocity of the flow that exits from the undercarriage is reduced with *Sealed gap*. Only minor changes can be observed along the trailer sides.

(a) Sealed gap

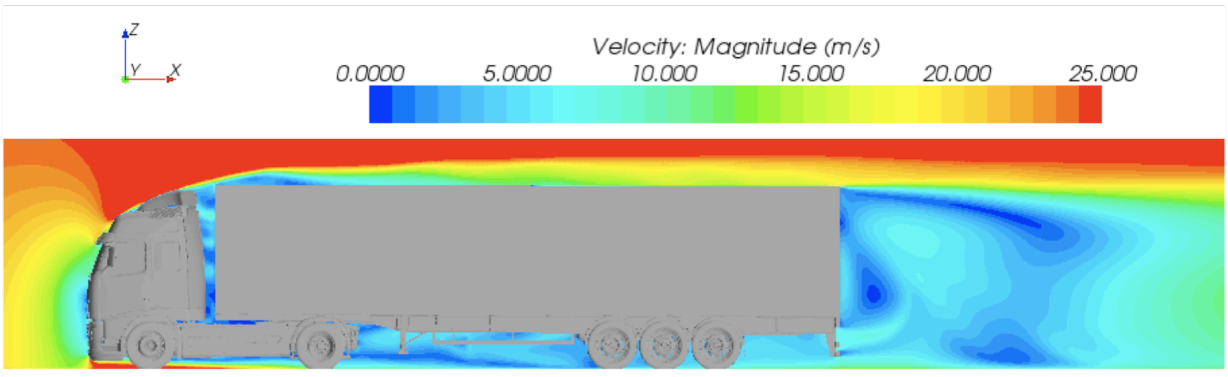

(b) Reference

Figure 25: The velocity magnitue around the truck, displayed in the symmetry plane, 0° yaw

In yaw conditions this configuration works very well; an improvement of 41 DC is achieved. Figure 26 shows the velocity differences on the leeward side and how the gap sealing improves the flow, especially on the roof and on the upper part of the side.

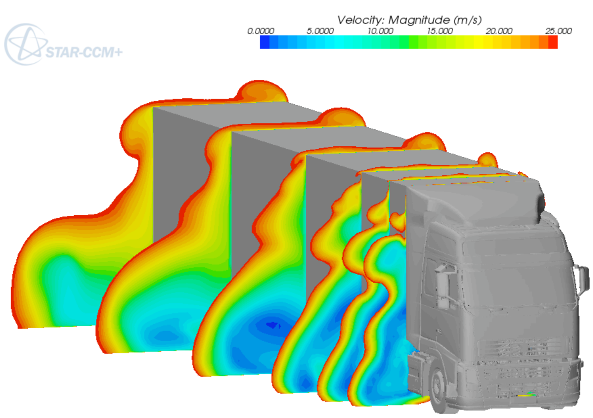

(a) Sealed gap

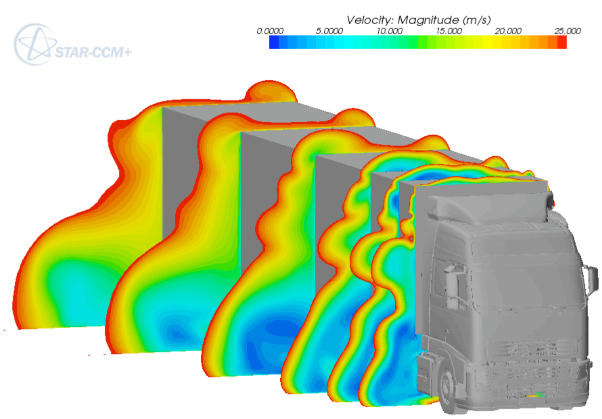

(b) Reference

Figure 26: The velocity magnitude on the leeward side, Sealed gap compared to the Reference, 5° yaw

4.2.2 Vortex stabilizer

As seen in Table 4, the *Vortex stabilizer* does not improve the results significantly. In 0° yaw, no improvement is achieved at all. The reason for this is seen when displaying the pressure coefficient on the trailer front face. When adding the *Vortex stabilizer* the pressure increases on the trailer front. When the air, coming into the gap from the sides, remains trapped by the stabilizer the pressure here increases, which is opposite the wanted effect. However, velocity magnitude displayed in different x-planes shows that a more symmetric flow is obtained along the trailer roof with the stabilizer in use.

Table 4: Change in drag with Vortex stabilizer

DC - 0° yaw	DC - 5° yaw	Weighted DC
1	-9	-6

When exposing the vehicle to yaw the *Vortex stabilizer* is more useful, an improvement of 9 DC is acquired. Here it prevents the cross-flow that otherwise occurs in the gap, and reduces the amount of air that exits and separates at the leeward side, Figure 27.

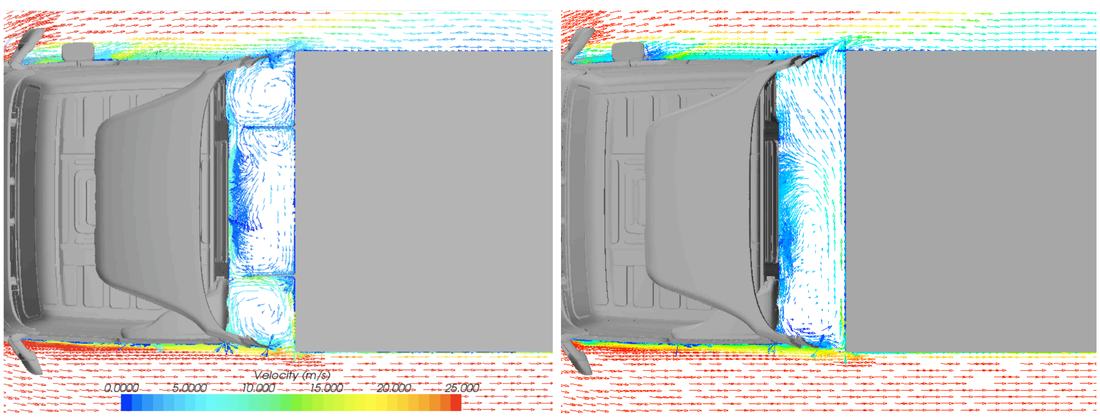

(a) Vortex stabilizer (b) Reference

Figure 27: Velocity vectors displayed in 1900 mm above ground, 5° yaw

4.2.3 Gap fairing

The results of drag changes with *Gap fairing* are seen in Table 5.

Table 5: Change in drag for Gap fairing

DC - 0° yaw	DC - 5° yaw	Weighted DC
-7	-20	-15

As can be seen in Table 5, *Gap fairing* reduces the drag with 15 DC. Figure 28 shows how *Gap fairing* enables a smoother flow over the gap, resulting in an improved flow attachment that reduces the low-velocity bubble at the top of the trailer front. The picture also shows how the pressure peaks at the upper corners and at the edges of the trailer front are reduced.

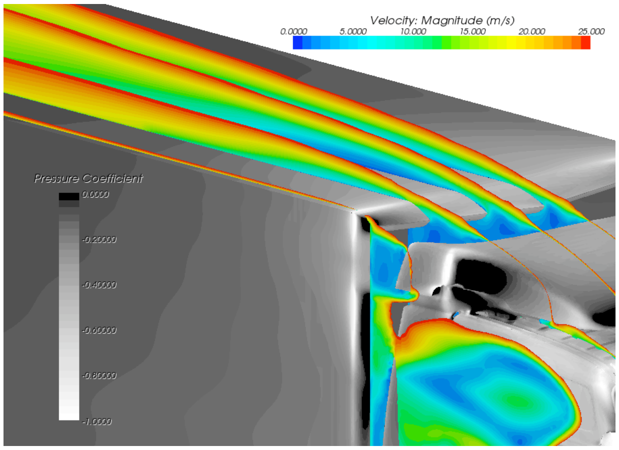

(a) Gap fairing

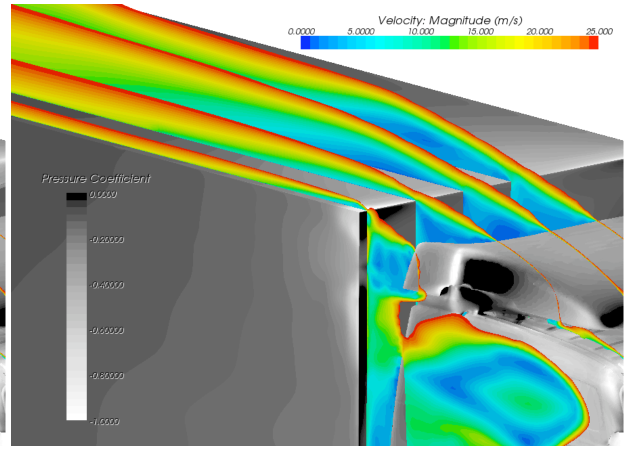

(b) Reference

Figure 28: Velocity magnitude in different y-planes, 0° yaw

The drag improvements in cross-wind conditions, 20 DC, can mostly be observed at the roof and on the leeward side of the trailer. Massflow calculations reveals that less air goes into the gap through the side clearance, compared to the *Reference*, reducing the disturbances. In addition, the streamlined edges on the trailer front reduce the flow separation and improve the flow attachment along the trailer surface. Figure 29 which shows how the drag accumulates along the truck, confirms that the drag is reduced in the gap region.

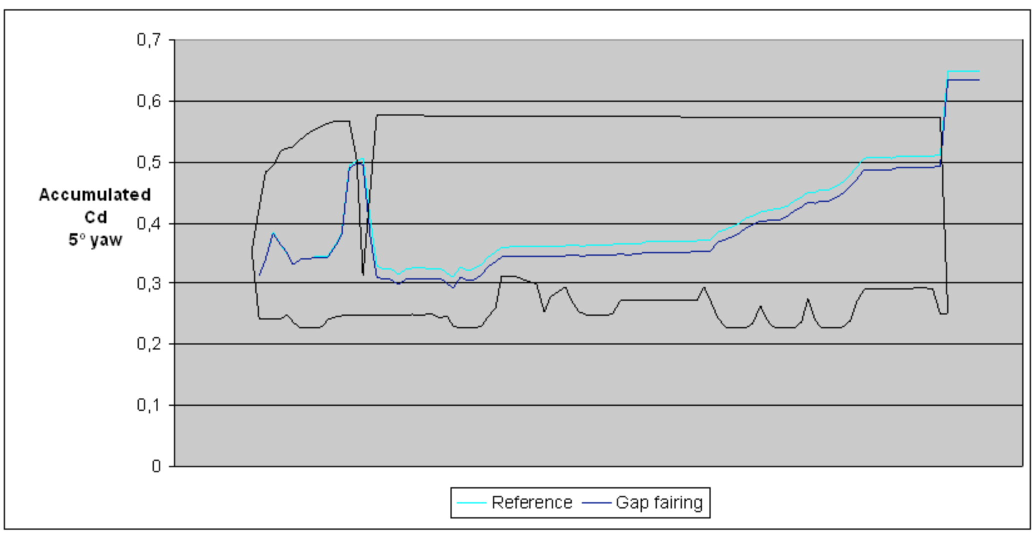

Figure 29: The accumulated drag along the truck in 5° yaw, Gap fairing compared to Reference

4.2.4 Side plates

As seen in Table 6, *Side plates* gives a drag improvement of 25 DC, weighted value. Pictures from the 0° yaw simulation show a reduced low-pressure acting on the trailer back along with a significant reduction of the base wake, see Figure 30. The angled *Side plates* guides the air towards the centre of the base wake, reducing the width of the wake. Due to the inward angle of the plates and that the air stays attached, the air is forced to accelerate and the plates experience a low-pressure on the outer side.

Table 6: Change in drag when adding Side plates

DC - 0° yaw	DC - 5° yaw	Weighted DC
-19	-28	-25

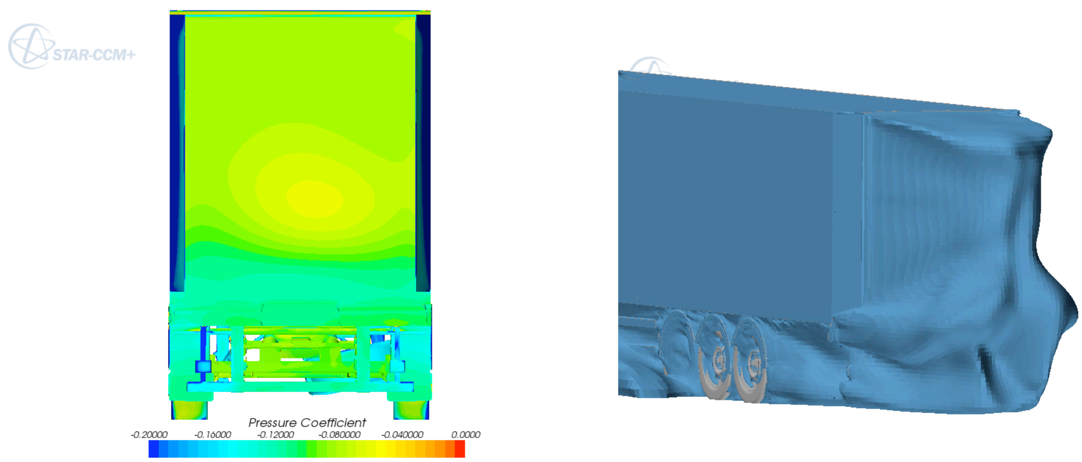

(a) Pressure coefficient on trailer back

(b) Iso surface of total pressure set to zero

Figure 30: The base region with Side plates in use, 0° yaw

In the 5° yaw case, the same improvements in the base wake are achieved and 28 DC are gained compared to the Reference case. Figure 31 illustrates the velocity vectors in the base wake, seen from above. The pictures clearly show how well the plates work in yaw condition and how the plates bring the air closer to the center and create a more symmetric wake.

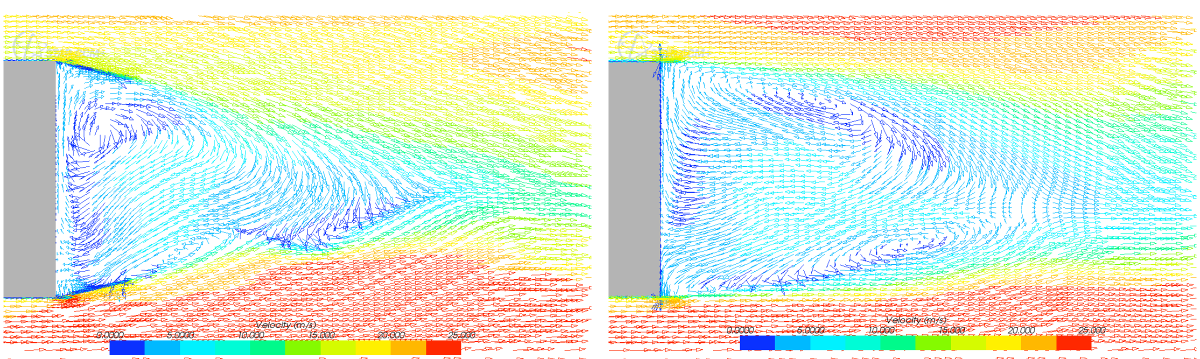

(a) Side plates

(b) Reference

Figure 31: Velocity vectors displayed in a z-plane 1900 mm above ground seen from above, 5° yaw

4.2.5 Base plates

The aim of adding the so-called *Base plates* is to decrease the base wake by guiding the air from the roof and the undercarriage to the center of the base wake. The improvements in drag counts are shown in Table 7.

Table 7: Change in drag when adding Base plates

DC - 0° yaw	DC - 5° yaw	Weighted DC
-14	-18	-16

The outcome of adding the *Base plates* is a higher pressure, although still a low-pressure, in the base wake that will decrease the pressure difference between the front and the rear. Pictures of the velocity vectors shows how the air stays attached over the edge of the trailer roof and along the upper base plate, see Figure 32. The airflow maintains in the direction of the plates and the picture shows a significant vertical contraction of the base wake.

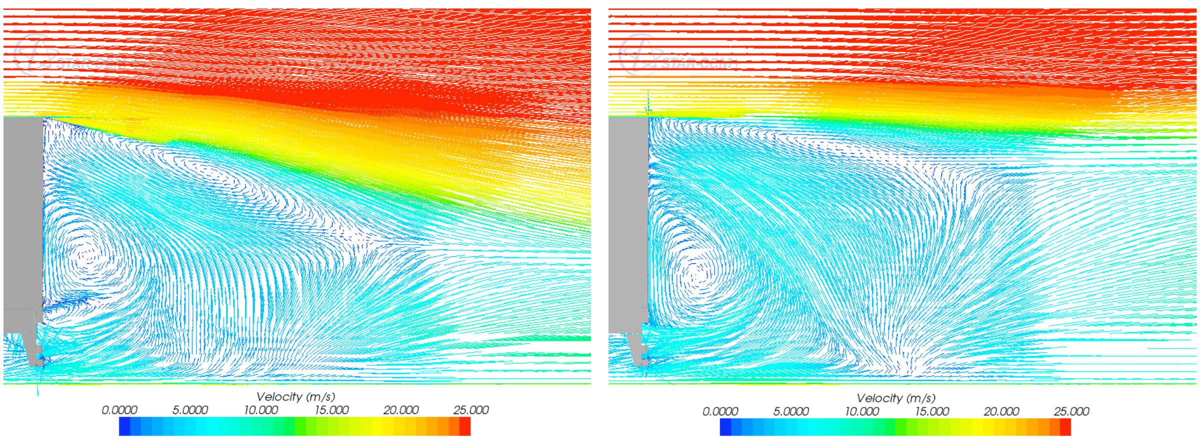

(a) Base plates (b) Reference

Figure 32: Velocity vectors of the base wake displayed in the symmetry plane, 0° yaw

The lower plate on the other hand is not as effective. Rear-light arrangement and other beams make it difficult for optimal placement. In addition, the flow is already very irregular and turbulent which makes it difficult to guide it. As can be seen in Figure 32, the air exiting under the trailer has a slightly lower velocity compared to the reference case. One reason for this could be the strong downwash from the upper plate that creates a blockage that retards the undercarriage flow and thus reduce the velocity. The reduced velocity, possible in combination with the lower plate, results in a steeper, although weaker, upwash.

The same effects are achieved in yaw conditions; a smaller base wake with less concentrated low-pressure regions.

4.2.6 Frame extension

When combining *Side plates* and *Base plates* the device *Frame extension* is obtained. This device has very good results in both 0° and 5° yaw, see Table 8.

Table 8: Change in drag for Frame extension

DC - 0° yaw	*DC* - 5° yaw	Weighted *DC*
-37	-56	-49

Figure 33 shows that the pressure distribution on the trailer back is almost uniform, except the low pressure acting on the plates due to acceleration. The mean pressure at the trailer back is definitely larger than the *Reference* case, which has a positive effect on drag. As seen in Figure 34, compared to the *Reference*, no significant low-pressure swirl is created behind the trailer back. The same effects, regarding a strong downwash and a poor upwash, which were achieved with *Base plates,* also applies for *Frame extension.*

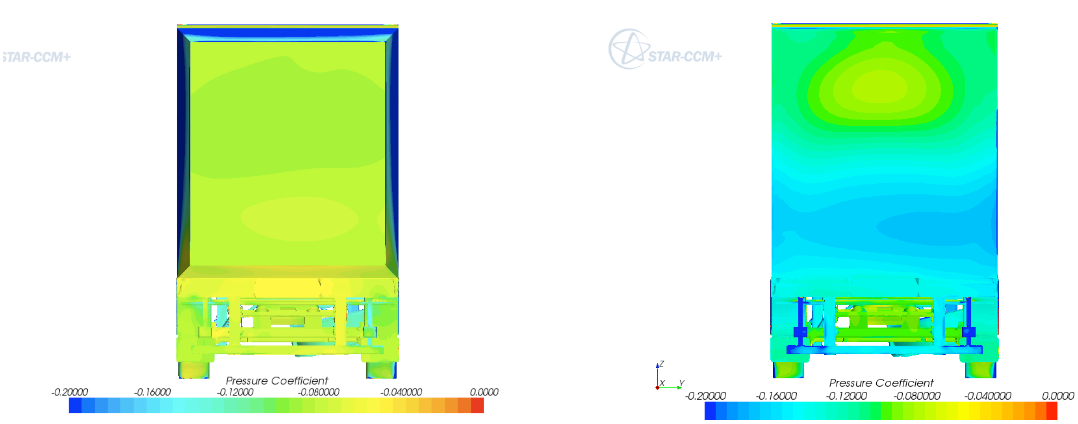

(a) Frame extension (b) Reference

Figure 33: Pressure coefficient displayed on the trailer back, 0° yaw

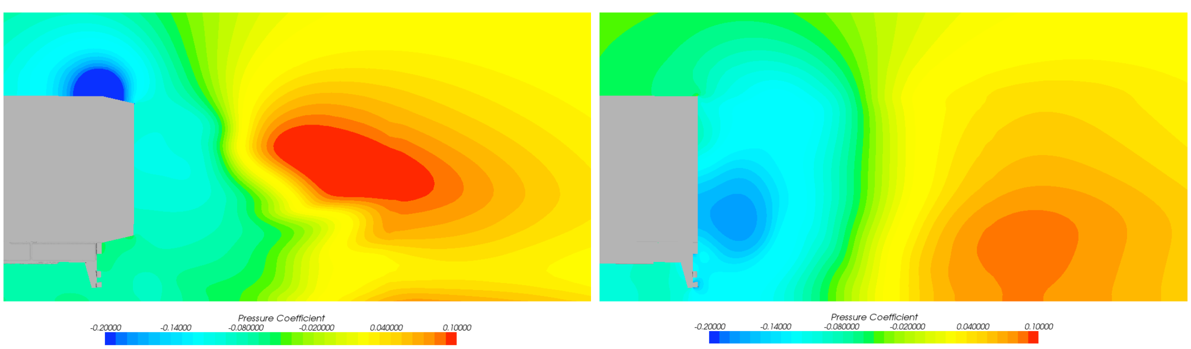

(a) Frame extension (b) Reference

Figure 34: Pressure coefficient displayed in symmetry plane, 0° yaw

The angle of the plates in *Frame extension,* especially the top plate and the two side plates, is very effective at guiding the air and reducing the base wake, in both yaw conditions. Figure 35 illustrates the base wake in 5° yaw, and the iso surface shows how the upper part of the wake is significantly reduced. The lower part on the other hand, is hardly affected at all. The same phenomenon that was achieved with *Base plates*, regarding blockage of the exit zone for the undercarriage flow, is also obtained with *Frame extension*.

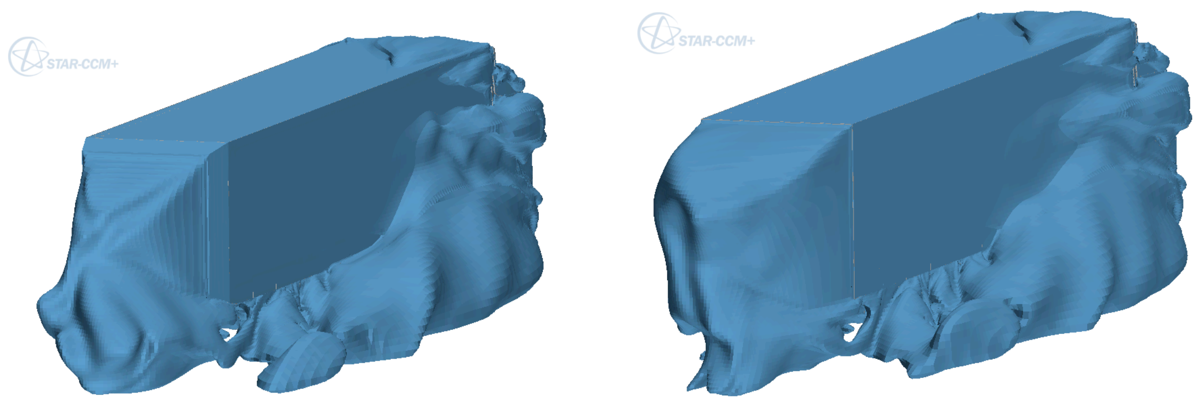

(a) Frame extension (b) Reference

Figure 35: Iso surfaces of total pressure equal to zero, 5° yaw

4.2.7 Side skirts

Results from simulations of *Side skirts* are seen in Table *9*. As seen in the table there is a tremendous improvement in 5° yaw. During 0° changes in the flow can mostly be observed along the trailer sides at ground level. Additionally, improvements can also be seen from the side diffuser at the rear; stabilizing the flow and directing it towards the center of the base wake.

Table 9: Change in drag for Side skirts

DC - 0° yaw	DC - 5° yaw	Weighted DC
-25	-102	-77

Figure 36a and 36b represent the velocity magnitude underneath the trailer with and without side skirts in 5° yaw. There is a great advantage with *Side skirts* in yaw condition where it prevents the undercarriage from cross-winds. It thereby reduces the flow disturbances underneath the trailer and directs the flow along the trailer side. The reduced amount of air entering the undercarriage is confirmed by the massflow calculations underneath the trailer, see the numbers in the same figures. In the open region in front of the trailer wheels there is a massflow of 6.9 kg/s for *Side skirts,* compared to 22.8 kg/s for *Reference*. It is also seen how the velocity in this region is significantly reduced.

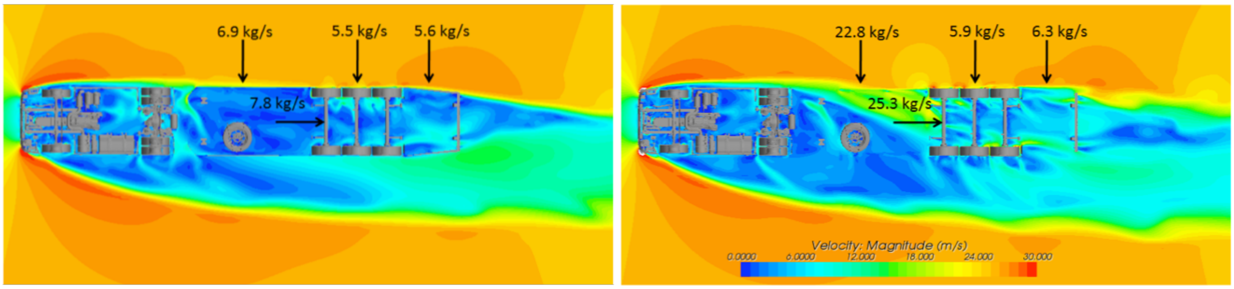

(a) Side skirts (b) Reference

Figure 36: Velocity magnitude under Side skirts and Reference with calculated massflow entering the undercarriage region, 5° yaw

The positive effect with *Side skirts* is also confirmed by comparing Figure 37a and 37b, visualizing the pressure distribution underneath the trailer. A large reduction of pressure is especially seen in the region around the wheels and wheel axles which reduces the pressure drag.

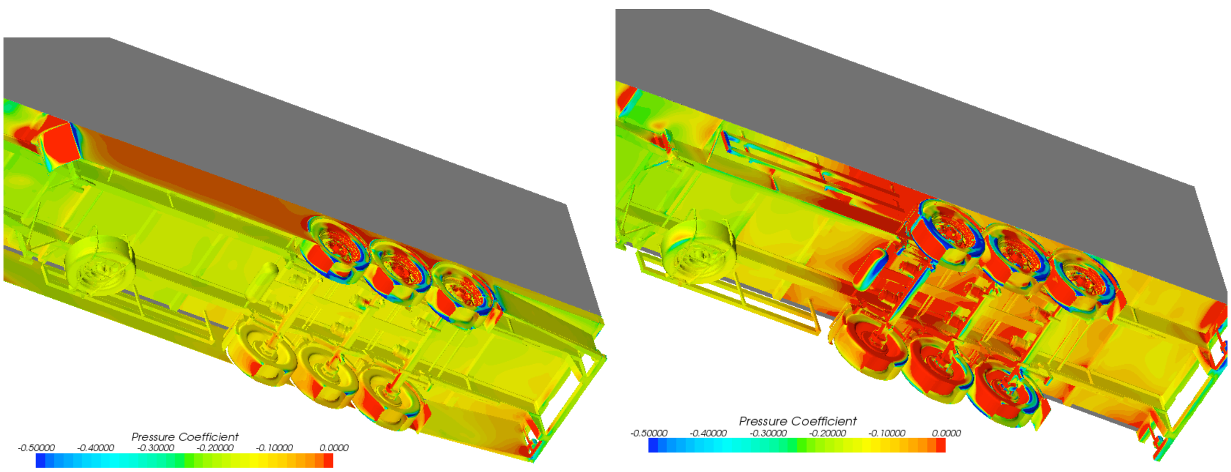

(a) Side skirts (b) Reference

Figure 37: Pressure coefficient displayed on the undercarriage of the trailer, 5° yaw

4.2.8 Smooth underbody

As seen in Table 10, almost all improvement with *Smooth underbody* is achieved during cross-wind conditions, 51 *DC*. In 0° yaw the effect of *Smooth underbody* is hardly notable. A larger velocity of the undercarriage flow can be seen at the rear together with an increased upwash.

Table 10: Change in drag for Smooth underbody

DC - 0° yaw	DC - 5° yaw	Weighted DC
-2	-51	-35

Figure 38 visualizes the velocity magnitude underneath the trailer and shows a significant increased undercarriage flow. Disturbances in the undercarriage flow are reduced since the irregular trailer underbody is covered by a smooth surface. Due to the narrower ground clearance under the wheel bogies, the velocity in this region is accelerated. Additionally, the rear diffuser increases the upwash and reduces the base wake.

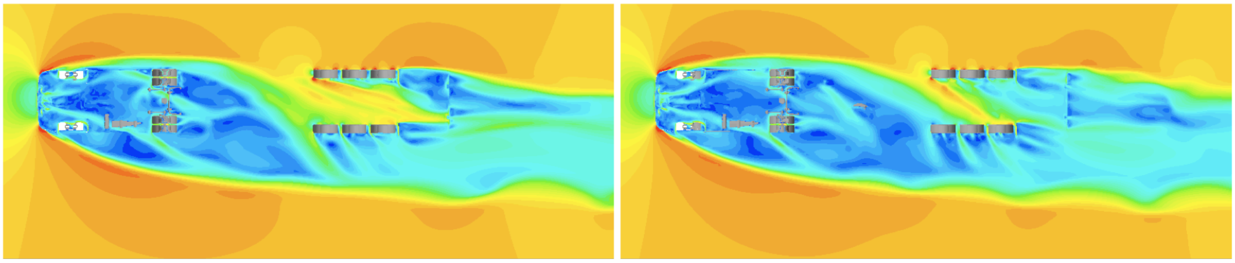

(a) Smooth underbody (b) Reference

Figure 38: Velocity magnitude displayed approximately 250 mm above ground, Smooth underbody compared to Reference, 5° yaw

4.2.9 Sealed wheels

In Table 11, the results of *Sealed wheels* are shown and large drag improvements can be found, especially in 5° yaw. As discussed in Subchapter 4.1, most of the air that enters the undercarriage in 0° yaw goes in from the trailer wheels and downstream, and when applying *Sealed wheels,* the drag is improved with 29 DC.

Table 11: Change in drag for Sealed wheels

DC - 0° yaw	DC - 5° yaw	Weighted DC
-29	-111	-83

Sealed wheels shows the same effect as *Side skirts*, although with further improvements around the wheels. From massflow calculations it is seen that less air enters and leaves through the wheels, resulting in a reduction of flow disturbances under the trailer. This is confirmed from pictures of the velocity magnitude under the trailer, representing a smoother and better attached flow along the wheels, see Figure 39.

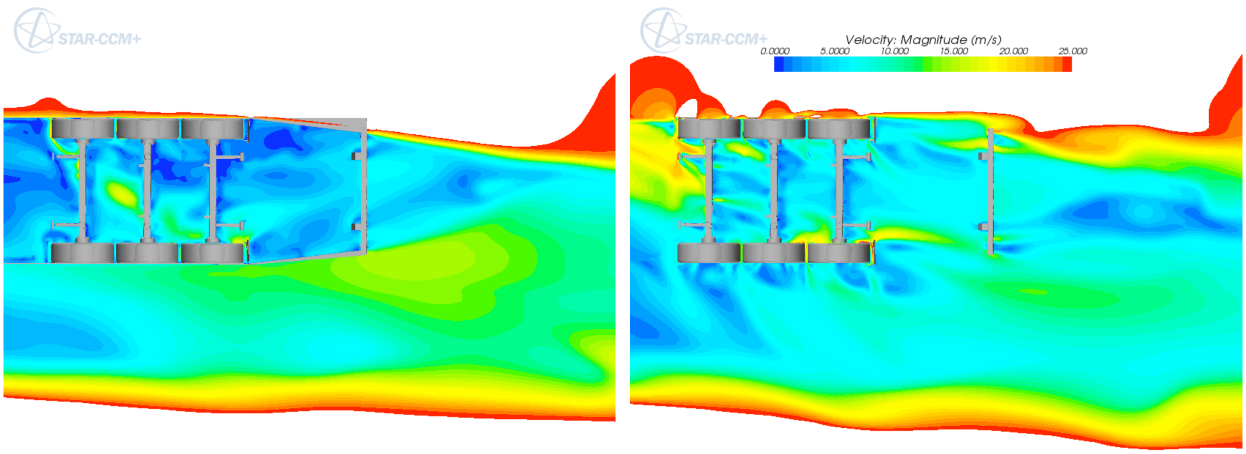

(a) Sealed wheels (b) Reference

Figure 39: Velocity magnitude in the z-plane, 500 mm above ground, trailer wheels region seen from underneath.

4.2.10 Teardrop

Due to the drop-shaped design of *Teardrop* in x-direction this configuration works best in 0° yaw; an improvement of 24 *DC* is achieved. In 5° yaw, changes in the flow structure are mostly seen in the base wake where a fairly strong downwash and thereby a reduced base wake is obtained. The increased side area retards the improvements, and on the leeward side of the trailer a slightly larger wake is observed, compared to the *Reference.*

Table 12: Change in drag for Teardrop

	DC - 0° yaw	*DC* - 5° yaw	Weighted *DC*
Teardrop	-24	-7	-13

When creating *Teardrop,* a half-meter of extra material is added on the roof of the trailer, which means that the frontal area of the truck is increased. However, to keep the result of *Teardrop* comparable to the *Reference* case, the same frontal area was used when calculating C_d.

Figure 40, representing the velocity magnitude in 0° yaw, shows that *Teardrop* gives an significant improvement of the flow along the roof of the trailer, compared to the *Reference.* Together with the slope at the rear, this results in a substantial downwash. In addition, the air that exits from the undercarriage has a reduced velocity, thus a decreased upwash.

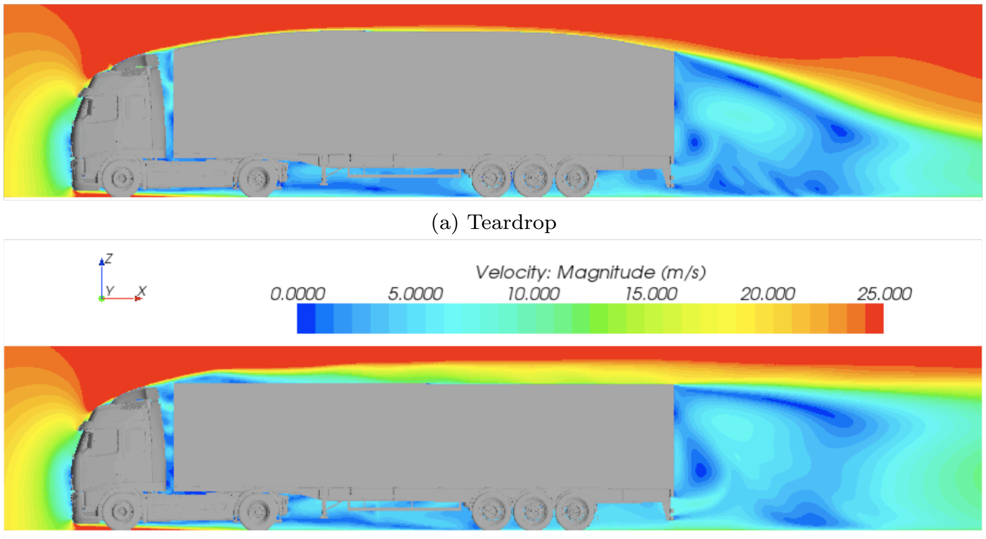

(a) Teardrop

(b) Reference case

Figure 40: Velocity magnitude displayed in symmetry plane, 0° yaw

The figure above also shows that *Teardrop* represents a good flow attachment over the gap. As the flow follows closer to the surface, from the tractor and downstream the trailer, more air is also being transported into the gap, which increase the disturbances of the flow in this region. The effect of this is shown in pictures of the pressure coefficient at the trailer front, indicating that *Teardrop* experience an increased pressure at upper part of the trailer front, compared to the *Reference*.

4.2.11 Basedrop

As seen in Table 13, the drop-shaped base of the trailer improves drag and gives a weighted value 37 DC.

Table 13: Change in drag for Basedrop

	DC - 0° yaw	DC - 5° yaw	Weighted DC
Basedrop	-20	-46	-37

In both yaw conditions, iso pictures shows how the wake structure of this configuration is very unbalanced. The upper part of the base wake has a very good transition from the trailer and follows the geometry well, creating a narrow base wake. The lower part, by contrast, is enlarged. This can be seen for 5° yaw in Figure 41. Pictures of the pressure distribution on the trailer back reveal an increased pressure with *Basedrop*, compared to the *Reference*, especially at the lower part.

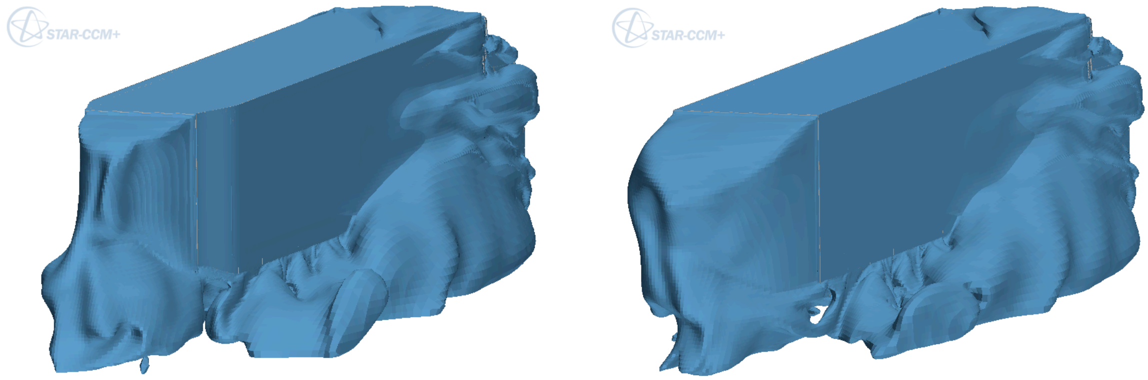

(a) Basedrop (b) Reference

Figure 41: Iso surfaces of total pressure equal to zero, Basedrop versus Reference in 5° yaw

4.3 Evaluation of individual devices and choice of combinations

In Figure 42, the weighted ΔC_d from the results of the individual devices is presented.

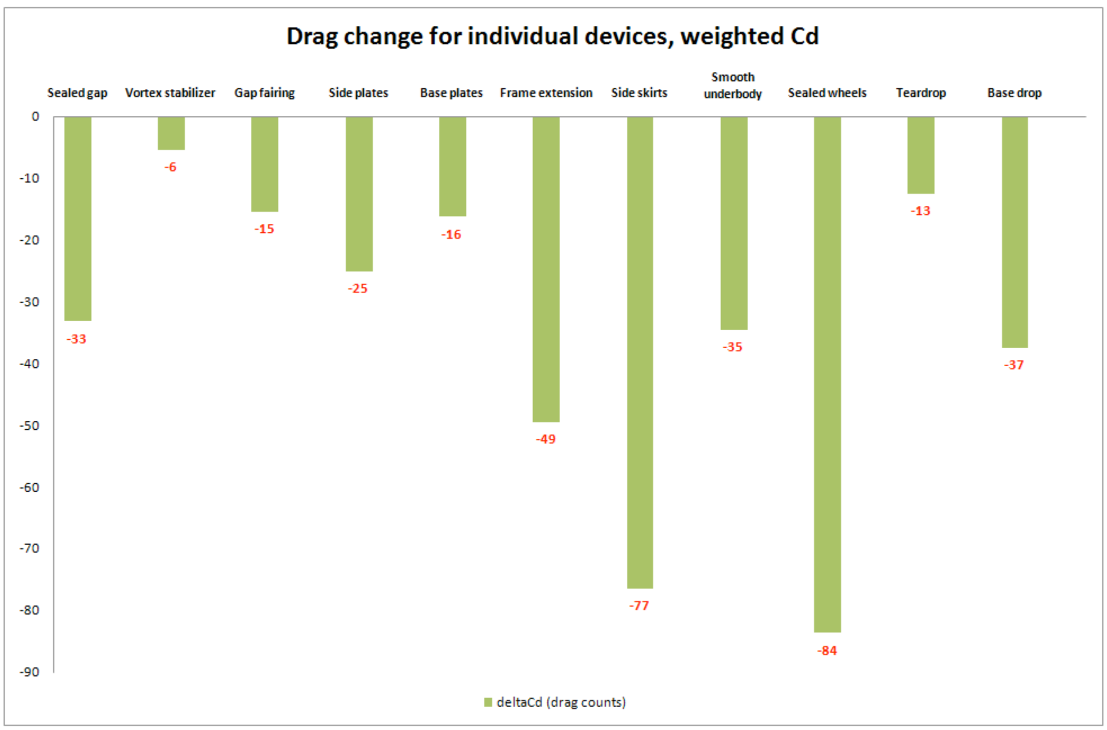

Figure 42: The weighted value of drag change.

As has been shown from the results, Figure 42, *Side skirts* and *Frame extension* gives the most significant drag improvements. This gives an indication that the airflow underneath the trailer and behind the trailer have a large influence on drag and that these regions are of great interest for further investigations.

Both *Smooth underbody* and *Sealed gap* gave fairly good results. However, these configurations were only tested to obtain an understanding of their influence on the drag and will not be used in the combinations. The same applies to *Sealed wheels;* the wheels cannot be covered without further consideration of cooling of the brakes.

Those devices with the aim of affecting the flow in the gap did not improve the drag significantly, except for *Sealed gap* that will be disregarded. However, a phenomenon that can be observed with both *Vortex stabilizer* and *Gap fairing* is how the flow along the roof is stabilized and more symmetric, something that follows the flow all the way to the base wake. The flow in the gap clearance is very irregular and chaotic and air is both entering and leaving the gap along the border. The air leaving the gap at the top zone, sometimes in the form of swirls, disturbs the flow and creates an unstable flow behavior. *Vortex stabilizer* helps the air leave the gap in a more controlled way, whereas *Gap fairing* prevents this unstable air to exit at the top and reduces the flow disturbances over the gap.

To achieve further improvements of drag by combining these devices, it is necessary to considered how they affect the flow and thereby the drag. Those devices that are placed at the rear of the trailer usually only affect the upper part of the base wake. It would thus be beneficial to combine these with a device that has an effect of the lower part of the base wake, for example *Side skirts.* A combination of two devices like this could result in a more symmetric and stable base wake that reduces the drag.

Figure 43 shows a chart of the accumulated drag along the truck with *Side plates, Base plates* and *Frame extension* in 0° yaw. The chart shows that the usage of *Base plates* and *Frame extension* in the base wake improves the drag already in the fore part of the trailer. *Frame extension* has a slightly lower drag along the whole trailer, although the major difference occurs in level with the trailer wheels and from there on improves the drag significantly.

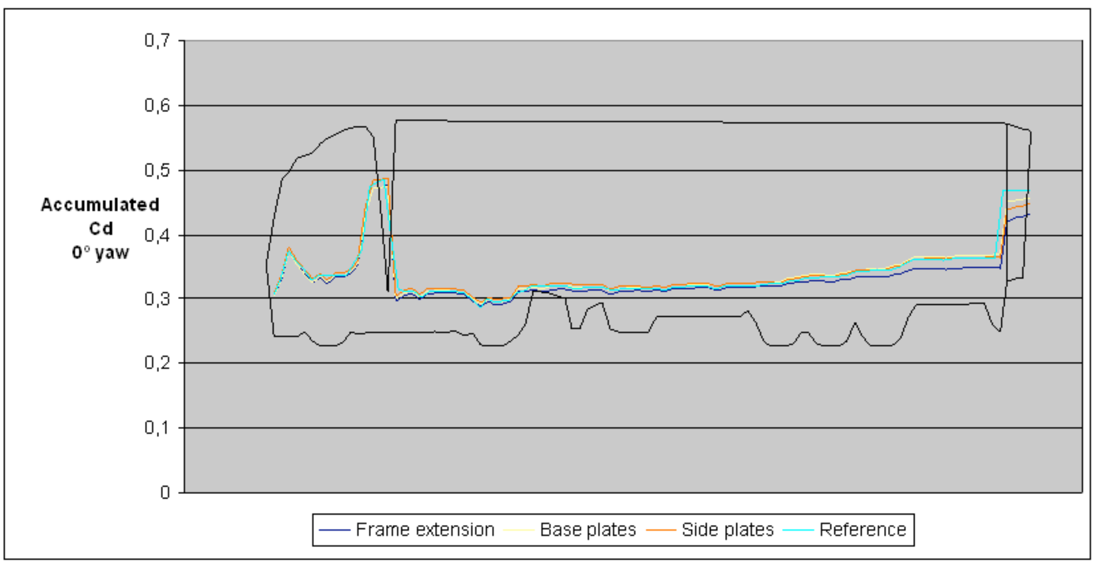

Figure 43: Accumulated drag along the truck with Side plate, Base plates and Frame extension, 0° yaw

The different devices tested to improve the flow underneath the trailer all gave very good results, especially in yaw conditions. The chart of how the accumulated drag increases along the truck in 5° yaw is illustrated in Figure 44. It is seen that these devices does not affect drag in the fore part of the truck. However, the picture shows how *Side skirts* and *Sealed wheels,* which have the same design up till the trailer wheels, actually increase drag with their first part that is bent inward. This part experience a high pressure in yaw and thereby increases the drag. The major gain in drag is obtained at the wheels where the *Reference* obtains a large part of its final drag value.

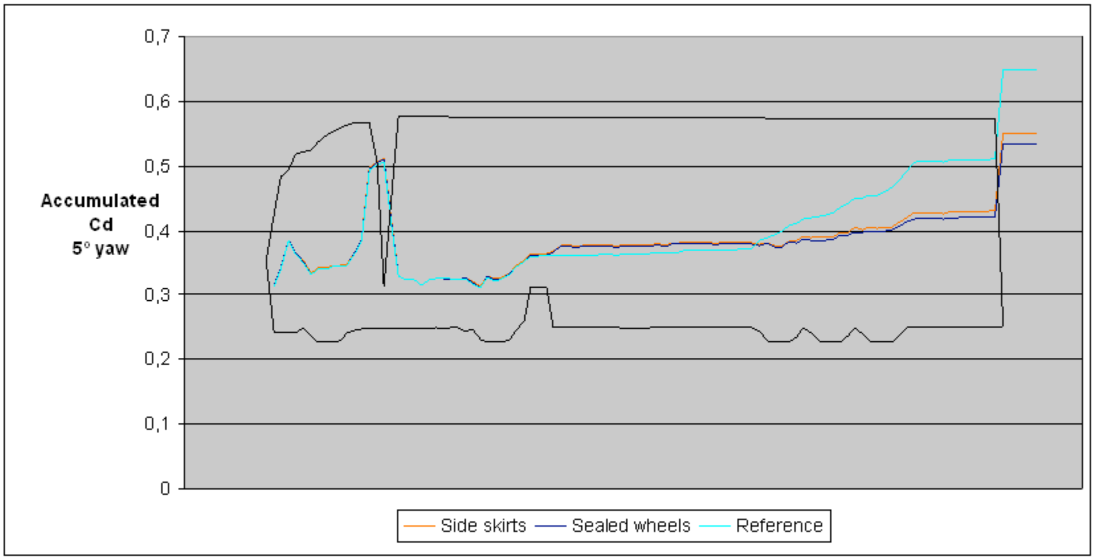

Figure 44: Side skirts and Sealed wheels compared to Reference, 5° yaw

At the rear of the trailer the boundary layer is fairly large. To improve the function of the devices in this region a thinner boundary layer would make it possible to affect more air and thereby increase the effect. The devices that do this, if disregarding *Sealed gap*, are *Gap faring* and *Teardrop*. Therefore it would be interesting to combine these two devices with *Frame extension*.

The combination *Teardrop* and *Side skirts* is interesting since these devices operate at their best in different yaw conditions, which can amplify the weighted result.

From the discussion above the following combinations have been chosen, see Table 14.

Table 14: Choice of combinations

Frame extension and Side skirts
Gap fairing and Frame extension
Gap fairing, Frame extension and Side skirts
Teardrop and Frame extension
Teardrop and Side skirts
Gap fairing, Frame extension, Side skirts and Teardrop

4.4 Results of combinations

The drag change in 0° and 5° yaw for the combinations can be seen in Figure 45. More details about the results for each combination are presented further down.

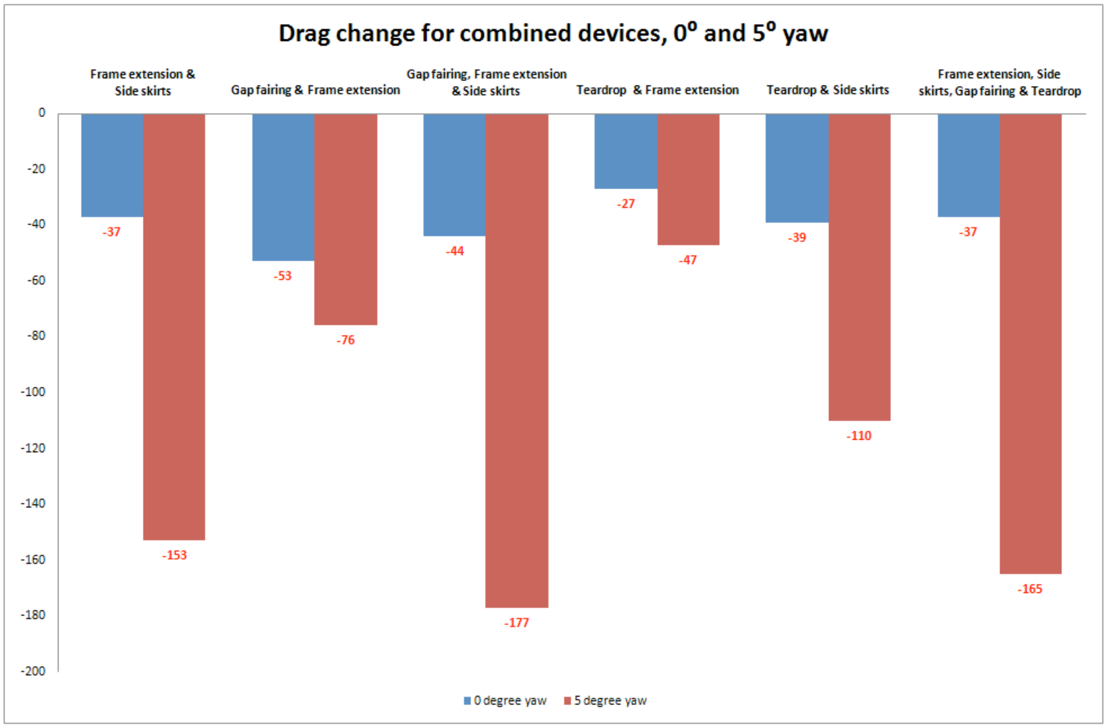

Figure 45: The results of the combinations in 0° and 5° yaw

4.4.1 Frame extension and Side skirts

The results of *Frame extension* combined with *Side skirts* can be seen in Table 15.

Table 15: Change in drag for Frame extension and Side skirts

	DC - 0° yaw	DC - 5° yaw	Weighted DC
Frame extension	-38	-54	-49
Side skirts	-26	-101	-76
Combined	**-37**	**-153**	**-114**

The combination of *Frame extension* and *Side skirts* did not improve the results in 0° yaw, compared to the single *Frame extension*. Pictures of the base wake structure shows that the wake is more compact with both devices in use and that the devices seem to compliment each other well. However, the pressure coefficient displayed on the rear face of the trailer reveals that a small and compact wake is not always better, see Figure 46. The reduced wake results in a more concentrated low-pressure acting on the rear face of the trailer which has a negative effect on drag.

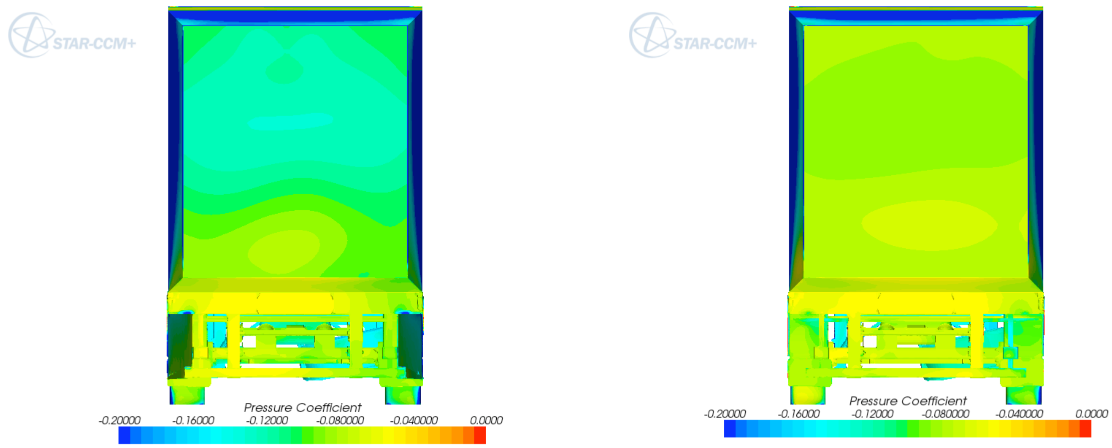

(a) Combination of Frame extension and Side skirts (b) Frame extension

Figure 46: Pressure coefficient at the trailer back, 0° yaw

Regarding yaw condition this combination achieves very good results. The combination obtains the advantages from each of the single device, which results in flow improvements at both the undercarriage and the base wake. This is confirmed from pictures of iso surfaces, showing a significant reduction of losses in the flow in these regions, see Figure 47.

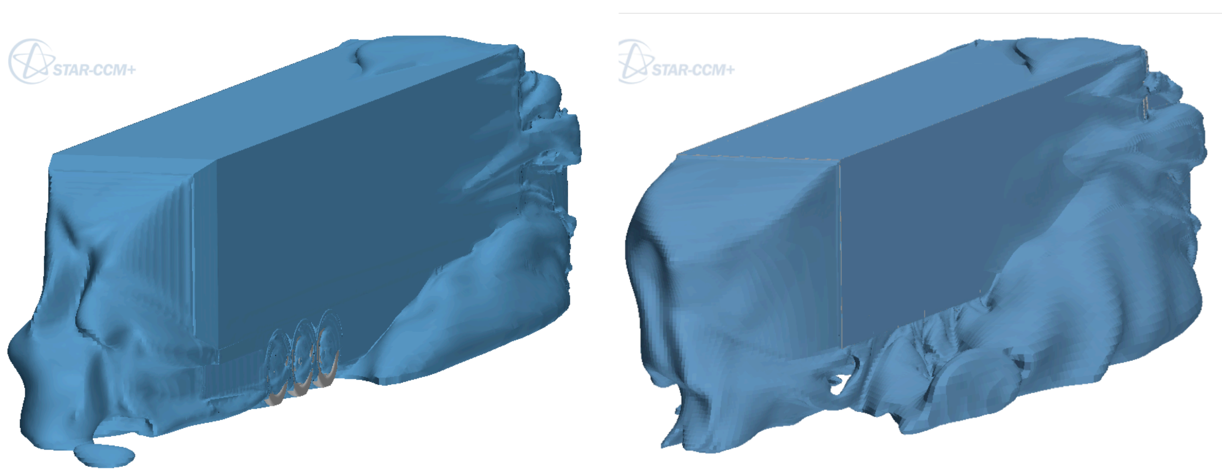

(a) Combination of Side skirts and Frame extension (b) Reference

Figure 47: Iso surfaces of total pressure equal to zero, 5° yaw

4.4.2 Gap fairing and Frame extension

The results of the combination *Gap fairing* and *Frame* extension are seen in Table 16. The result in 0° yaw needs to be considered with care since this simulation did not converge as good as the other.

Table 16: Change in drag for the combination Gap fairing and Frame extension

	DC - 0° yaw	DC - 5° yaw	Weighted DC
Gap fairing	-8	-19	-15
Frame extension	-38	-54	-49
Combined	**-53**	**-76**	**-68**

Pictures of iso surfaces for this combination shows that it has inherit the good features from the two devices, resulting in a reduction of the base wake and the wake at the fore part of the trailer roof. The flow is also more symmetric along the roof, a flow improvement obtained from *Gap fairing*. Additionally, as illustrated in Figure 48, the effect of the combination *Gap fairing* and *Frame extension* is a reduced boundary layer along the trailer roof, compared to *Gap fairing* alone.

(a) Frame extension

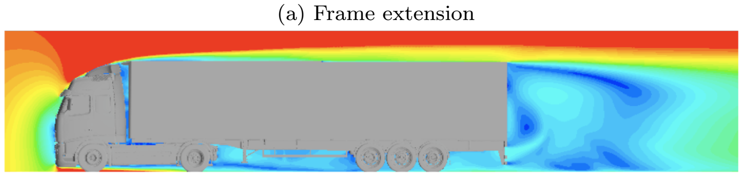

(b) Gap fairing

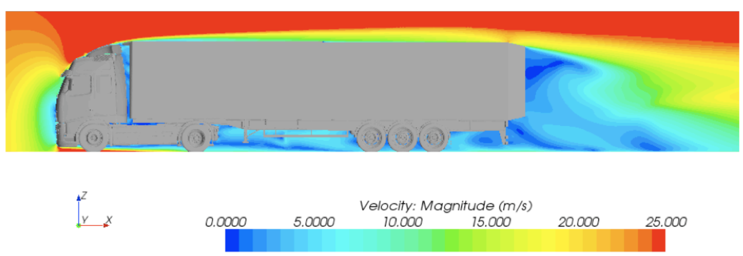

(c) Combination of Gap fairing and Frame extension

Figure 48: Velocity magnitude in the symmetry plane, 0° yaw

In 5° yaw, the same flow improvements applies for the combination as in 0° yaw. A better flow attachment over the gap together with a reduction of the base wake results in a drag improvement of 76 *DC*.

4.4.3 Gap fairing, Frame extension and Side skirts

The combination of *Gap fairing*, *Frame extension* and *Side skirts* gives a magnificent improvement of drag, especially during cross-wind conditions, 177 *DC*. The result confirms their different skills in the three main drag contributing regions; the gap, the undercarriage and the base wake. Improvements are also achieved in 0° yaw, although no large difference compared to the single *Frame extension*.

Table 17: Change in drag for the combination Gap fairing, Frame extension and Side skirts

	DC - 0° yaw	DC - 5° yaw	Weighted DC
Gap fairing	-8	-20	-15
Frame extension	-37	-56	-49
Side skirts	-25	-102	-77
Combined	**-44**	**-177**	**-133**

Iso pictures show a compact and symmetric base wake, together with a reduced wake structure along the trailer side and at the front of the trailer roof. The improved wake structure around the truck in 5° yaw, compared to the *Reference*, can be seen in Figure 49.

(a) Combination of Gap fairing, Frame extension and Side skirts

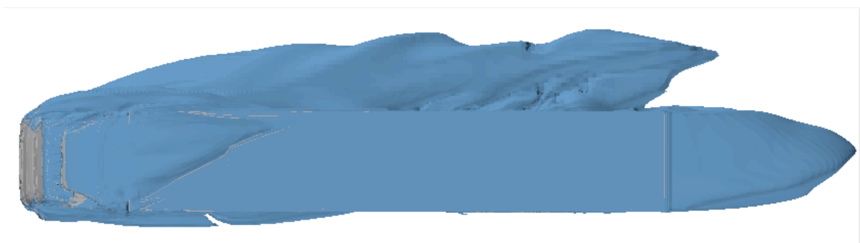

(b) Reference

Figure 49: Iso surfaces of total pressure equal to zero seen from above, 5° yaw

4.4.4 Teardrop and Frame extension

From Table 18 it is obvious that the combination of *Teardrop* and *Frame extension* does not result in any further improvements compared to *Frame extension* alone. Even though the combination shows a significant drag reduction in 5° yaw and a small reduction in 0° yaw, the individual *Frame extension* still shows the best result in both yaw cases.

Table 18: Change in drag for combination Teardrop-Frame extension

	DC - 0° yaw	DC - 5° yaw	Weighted DC
Teardrop	-25	-7	-13
Frame extension	-37	-56	-49
Combined	**-27**	**-47**	**-40**

Figure 50visualizes velocity vectors in the symmetry plane behind the trailer. Both *Teardrop* and *Frame extension* as single devices show a significant downwash behind the trailer, and by combining them an even stronger downwash is achieved. The teardrop-shaped trailer reduces the boundary layer along the roof and the effect of *Frame extension* is amplified, which results in a strong downwash. Although, the downwash is strong and steep, hence re-circulates into the undercarriage of the trailer, towards the flow direction. This flow phenomenon disturbs the undercarriage flow and reduces the poor upwash even more, making the base wake structure more unbalanced.

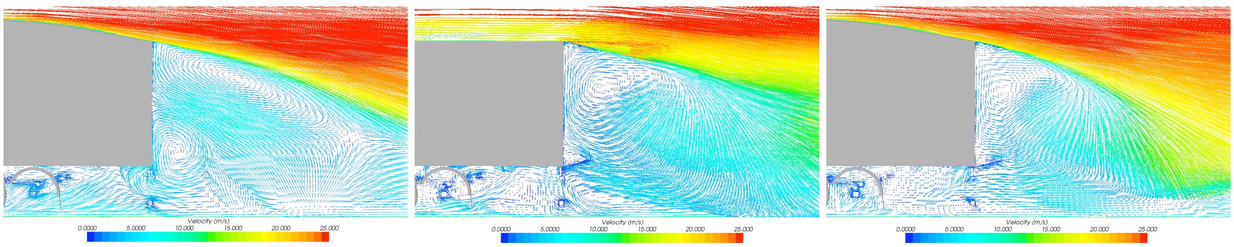

(a) Teardrop (b) Frame extension (c) Combination of Teardrop and Frame extension

Figure 50: Velocity vectors in the symmetry plane at the rear of the trailer, 0° yaw

During cross-wind conditions, pictures of iso contours of the flow structure around the combination indicate an increased wake at the leeward side of the trailer compared to *Frame extension*.

4.4.5 Teardrop and Side skirts

Table 19 shows the drag changes when combining *Tear drop* and *Side skirts*. Compared to the individual devices, the combination gives a fairly good improvement of drag in 0° yaw. During cross-wind conditions a large drag reduction is achieved with the combination, compared to *Teardrop*, although a small drag improvement compared to *Side skirt*s.

Table 19: Change in drag for combination Teardrop and Side skirts

	DC - 0° yaw	*DC* - 5° yaw	Weighted *DC*
Teardrop	-25	-7	-13
Side skirts	-26	-101	-76
Combined	**-39**	**-110**	**-87**

As seen in Figure 51, the combination utilizes the effect from the teardrop-shaped trailer and together with an improved flow attachment along the trailer skirts this results in a reduction of drag in 0° yaw. Pictures of iso contours confirm a reduction of losses in the flow at the front roof of the trailer, along the sides of the trailer at ground level and in the base wake. From pictures of velocity vectors of the base wake it is also seen how the combination reduces the low-pressure swirl at the lower part of the trailer back. Together with an even stronger downwash the base wake structure is slightly reduced.

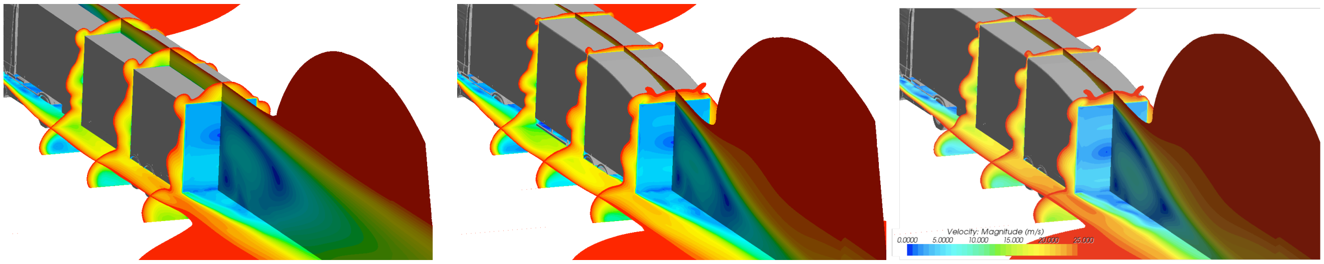

(a) Side skirts (b) Teardrop (c) Combination of Side skirts and Teardrop

Figure 51: Velocity magnitude displayed in the symmetry plane, a z-plane 150 mm above ground and in different x-planes, 0° yaw

In 5° yaw, the combination shows a small improvement of drag. The significant effect from *Side* skirts is obvious while *Teardrop* has a quite weak contribution to drag improvements during yaw conditions.

4.4.6 Gap fairing, Frame extension, Side skirts and Teardrop

By combining *Gap* fairing, *Frame extension, Side skirts* and *Teardrop*, the drag contributing areas around the truck are covered. However, Table 20 reveals that the drag improvement in 0° yaw is no greater than the individual *Frame extension*. From pictures of the pressure distribution at the trailer back, it is seen that *Frame extension* alone results in a better base wake pressure than the combination does. This is due to that *Teardrop* in the combination improves the flow along the roof and thereby reduces the pressure in the base wake.

Table 20: Change in drag for the combination Gap fairing, Frame extension, Side skirts and Teardrop

	DC - 0° yaw	DC - 5° yaw	Weighted DC
Gap fairing	-8	-19	-15
Frame extension	-38	-54	-49
Side skirts	-26	-101	-76
Teardrop	-25	-7	-13
Combined	**-37**	**-165**	**-122**

Compared to the *Reference*, the combination results in flow improvements over the gap, in the base wake, along the trailer roof and along the trailer sides in 5° yaw, see Figure 52, which gives a significant drag improvement of 165 DC.

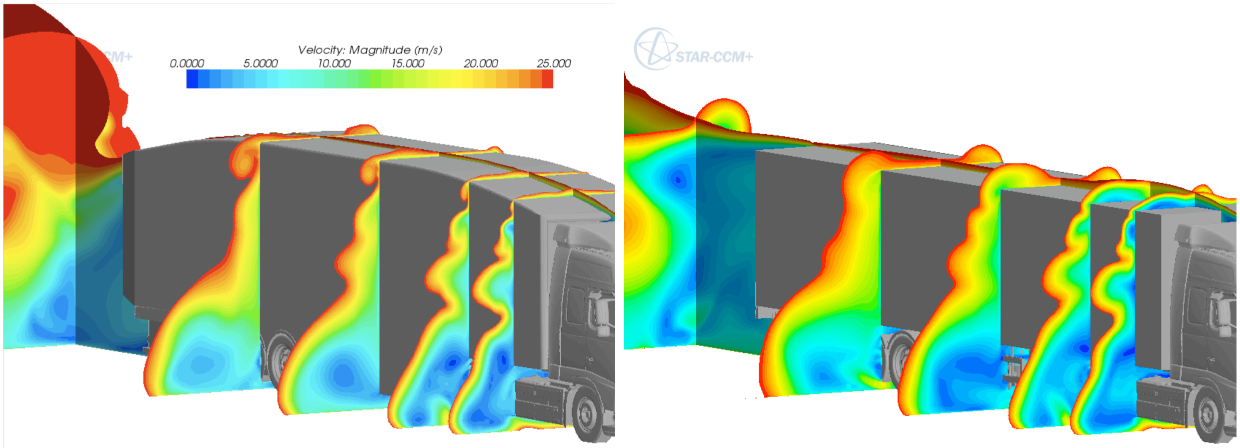

(a) Combination of Gap fairing, Frame extension, Side skirts and Teardrop

(b) The Reference

Figure 52: Velocity magnitude in the symmetry plane and in different x-planes along the truck, 5° yaw

4.4.7 Summary of the combinations

Figure 53 shows the weighted results from the combinations.

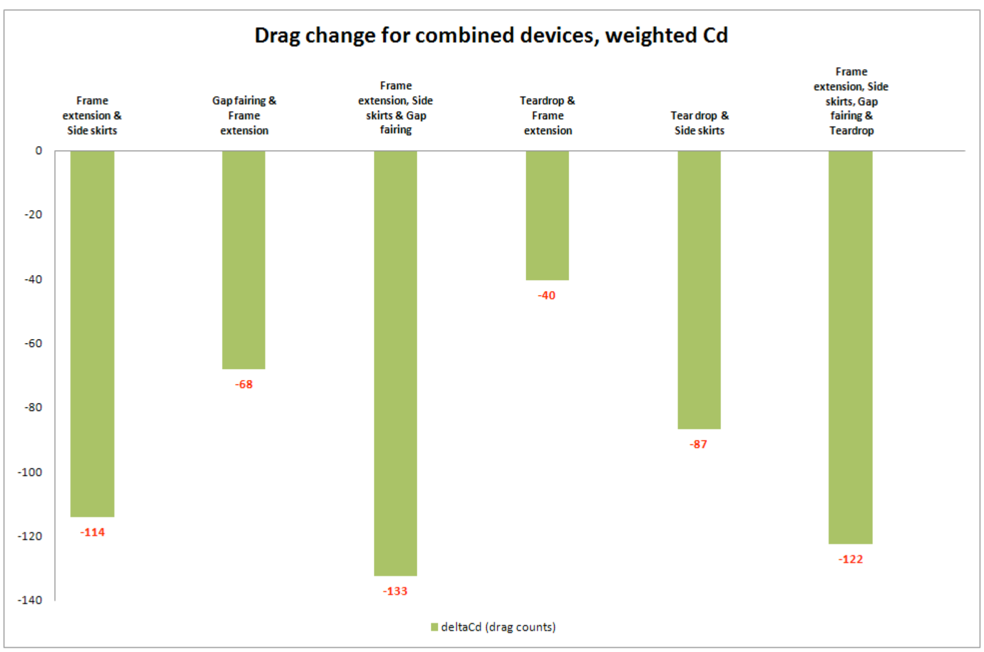

Figure 53: DC for the combinations

5 Discussion

As mentioned in Subchapter 1.1, an aerodynamic adjustment on the tractor alone can, in a successful case, give up to 1 or 2% drag improvement with today's design. During this project the average improvment of the individual trailer devices is 6%, without optimization. By combining several devices, drag improvements of up to 22% was achieved. These results give an indication of how much more drag there is to gain on the trailer compared to the tractor. Several examples have also been observed where an integrated development of the tractor and the trailer would smooth the transition of the flow between the two components, and thereby improve the results even more. In order to optimize the flow around the truck it is important to remember that velocity and pressure affects the flow upstream, which means that an adjustment in one region can affect other regions as well. From the simulations it is for example seen that adjustments at the rear of the trailer affects the flow all the way up to the gap region. This needs to be kept in mind when implementing a device at the rear. Naturally, the ideal procedure is to first optimize the vehicle in the front and then downstreams.

Sealed gap, Sealed wheels and *Smooth underbody* are devices that have been tested to see the drag contribution and the potential drag reduction in certain areas around the truck. These devices have great potential, although, further research and development are needed before implementation can be performed. *Sealed gap,* for example, is not designed with consideration to turning ability. However, *Sealed gap* gives a good guideline of how much the gap contributes to the total drag. In this project the drag from the gap only comprises about a few percent of the total drag, thus the effect of the gap treatments is not that substantial. However, the effect would probably increase if the gap or height difference between tractor and trailer was larger, since the device then would affect more air. It would nevertheless be interesting to see how close to the result of *Sealed gap* it is possible to come by designing the trailer and the tractor together. This would make it possible to optimize a device, such as *Gap fairing* for example, together with the roof- and side deflector on the tractor, in order to minimize the gap clearance and the drag contribution. The importance of adapting the tractor and the trailer to each other also applies for *Smooth underbody.* It is very difficult to obtain control over an already separated and turbulent flow, which is the case if a smoothed underbody is applied to the trailer and not to the tractor. The flow will then already be disturbed when reaching the trailer and the effect would not be as significant. Finally, research of how a fully closure of the undercarriage influences the cooling effect of the brakes, as less air enters this region, is required before *Sealed wheels* can be implemented. This device together with *Side skirts* shows the influence of the rotating wheels. The results show that covering the wheels improves drag with 7 *DC* compared to *Side skirts,* which is not as significant as expected. This could be due to the already improved flow and reduced losses achieved by the *Side skirts*.

As mentioned, *Frame extension* and *Side skirts* give the best result of the individual devices. Their drag reduction of 49 and 77 *DC*, respectively, corresponds to a reduction of fuel consumption with 2.5 % and 4.5 %, according to Equation 8. Furthermore, *Frame extension* combined with *Side skirts* is the best two-device combination, 114 *DC*, and shows almost equivalent result as when all the selected devices are combined together. These result reveals that the undercarriage and the base flow are very susceptible for improvements; changes in these regions can have significant effect on the total drag.

The efficiency of the devices is varying depending on the yaw conditions. From simulations in 0° yaw it is seen that the effect of the undercarriage and gap treatment is rather poor, compared to 5° yaw where the improvements are vast. During cross-wind condition, a larger amount of air enters these regions, which increase the possibility for the devices to improve the flow. For the devices placed in the base wake, the difference between the two yaw conditions is not as large since the flow structure does not change as much.

By changing the geometry of the trailer to a more aerodynamic shape, a more beneficial flow around the truck can be achieved. Although, the *Teardrop* in this project did not even come close to the level of fuel saving of 10 % that was mentioned in Chapter 1. This can be explained by the fact that no changes was allowed to be made on the tractor. To obtain the maximum effect of such quite substantial change of the trailer, the tractor must be involved in the design of the trailer in order to obtain the desired flow over the gap and along the roof. *Basedrop* is another configuration where the geometry of the trailer has been modified. However, *Basedrop* means a decreased load volume that must be gained in drag counts for the configuration to be economically profitable. Compared to *Side plates*, which has the same functionality and is considerably easier to implement without reducing the load volume, *Basedrop* only improve drag with approximately 10 more drag counts. These are factors that need to be considered when comparing devices like this and the result indicates that it might not be beneficial to sacrifice one pallet of the trailer load in order to reduce drag.

To reduce drag, a symmetric base wake, horizontal and vertical, is desirable. For 0° yaw it is not a problem to reduce the wake symmetrically from the trailer sides, whereas the airflows from the roof and the undercarriage is more difficult to synchronize. Since the flow at the upper part of the trailer is less disturbed than the flow at ground level, the same treatment does not affect these areas equally. Hence, when a device like *Frame extension* is implemented at the rear of the trailer, the wake does not become symmetric. The air at the upper part of the trailer is well affected, whereas the flow at ground level is too chaotic to be improved. A significant downwash together with a retarded upwash creates an asymmetric wake in the vertical direction. These differences in the base wake structure are seen in the simulations of *Side plates* and *Base plates* and are confirmed by their drag improvements, *Side plates* has an advantage of 9 *DC* compared to *Base plates*. To improve the base wake structure it could be beneficial to use a diffuser at the rear of the trailer together with a smoother underbody in order to increase the poor upwash. Due to the disturbed undercarriage flow, it would be interesting to test how the result of *Frame extension* and *Base plates* would change if the lower plate was removed. Removing one plate would simplify the devices and probably still give a rather large drag improvement.

The results of the combinations show that substantial drag improvements can be achieved by combining devices. However, the devices have only been added together, without being adapted to each other and no consideration has been taken to achieve the optimal design of the combinations, for example the rough transition between *Teardrop* and *Frame extension*. Hence, further drag improvements of the combinations should be possible.

The combination *Frame extension, Gap fairing* and *Side skirts* is the best drag reducing configuration with a drag improvement of 133 *DC*. This corresponds to a fuel saving of about 7 percent. Although, when adding the teardrop-shaped trailer to this combination, the drag improvement is reduced. As seen from the results and the flow around the truck in Chapter 4, this combination is deteriorated in both yaw conditions. The same negative effect is also observed when combining *Teardrop* and *Frame extension*. The total performance is reduced as the disturbances in the base wake increase, due to the poor interaction between *Frame extension* and *Teardrop*. These results thus confirm the importance of evaluating the flow around the truck for each individual device before they are combined.

As mentioned in Chapter 2, a full-scale wind-tunnel test, conducted at the National Research Council of Canada (NRC) [9], was performed on trailer devices similar to *Frame extension, Side skirts* and *Vortex stabilizer*. Both *Frame extension* (49 DC) and *Vortex stabilizer* (6 DC) tested in this project, show equivalent improvements as the devices in the wind-tunnel test, 51 and 2 DC respectively. *Side skirts* in this project, on the other hand, gives a much larger drag improvement compared to the wind-tunnel result, 77 DC compared to 48 DC. This is probably due to their differences in design and that moving ground was not used in the wind-tunnel test. Additionally, another study was recently conducted at Langley Full Scale Tunnel in co-operation with SOLUS Solutions and Technologies and Old Dominion University [8]. A 1/4 scale model of a conventional truck and trailer devices similar to *Sealed wheels*, *Frame extension* and *Sealed Gap* were tested. The improvements from the tests, with a speed of 90 km/h and over a yaw sweep to calculate the wind average, are very close to the improvements of the same devices in this project. *Sealed wheels*: 97 versus 84 DC, *Frame extension*: 57 versus 49 DC and *Sealed gap*: 39 versus 33 DC (wind-tunnel versus CFD).

However, even though the results are quite similar, the comparability between these $\Delta C_d - values$ should be considered with care. CFD-simulations and wind-tunnel tests are two different methods where different factors influence the results. It is nevertheless interesting to see if the tendencies are the same, which they are in this case.

5.1 Uncertainty issues

When working with CFD simulations it is important to remember that the results are calculated approximations of a real airflow and that assumptions has been made in order to solve the flow equations. Additionally, RANS time-averages and simulates a steady state approximation of the time dependent turbulent flow. These are all approximations that affect and diminish the accuracy of the results, which needs to be kept in mind. However, even if the numbers presented in this report should to be considered with care, the same method is used for all cases which makes the cases comparable. The result gives a guideline of the tendencies in the flow behavior and where the major drag can be gained.

In the residual plots, it is seen that adjustments at the rear edge of the trailer sides affects the continuity. Compared to the *Reference* and other configurations the continuity residual increases from approximately 0.0007 to about 0.003 for 0° yaw simulations when these changes are made. This could be due that adjustments here results in an indistinct separation of the flow and thereby mass fluctuations in the base wake that goes from side to side. The base wake also changes shape all the time in meaning of wakes that grow and then release from the truck.

The result of the simulation is also affected by the mesh quality. To be able to achieve comparable results of the cases the mesh should be equivalent. However, due to the devices, with different placement and mesh resolution, the mesh differs. The amount of cells varies from $40 - 43$ million cells between the different configurations, meaning that some configurations resolve specific areas more than others. To keep the comparability between 0° and 5° yaw, and to save time, the mesh was not changed between these yaw cases. From an accuracy point of view, it would have been desirable to improve the resolution at the leeward side of the trailer during 5° yaw where the wake stretches outside the refinement box. The number of prism layers used can also be discussed. To resolve the boundary layer closest to the surface properly, the company behind STARCCM+ recommends about 10-12 layers, although in this project only 2 and 6 layers have been used due to computer capability and time limitation.

As mentioned in Subchapter 2.3.2, the hexahedral mesh is suitable for simulations with a dominant flow direction. This only applies if the faces are placed perpendicular to the flow. This means that it would have been preferable to adapt the mesh to the flow direction in 5° yaw.

6 Conclusions

This thesis verifies the possibilities of improving the aerodynamics around a truck in order to reduce the fuel consumption, and concludes that:

- Aerodynamic trailer devices have a great potential of reducing drag. Compared to the tractor, the trailer is much more susceptible for aerodynamic drag improvements and thus the fuel consumption can be substantially reduced by using trailer devices. By combining the devices, even larger drag improvements can be achieved.
- The undercarriage and the base of the truck are the two regions where the greatest effects are achieved when adding aerodynamic devices to the trailer.The devices *Side skirts* and *Frame extension* have during this project shown a large potential to improve the flow in these regions and should be of great interest for further development.
- It is not beneficial to aerodynamically change the geometry of the trailer since there are relative simple add-on devices that shows the equivalent effect.
- As mentioned in Chapter 1, the tractor at Volvo already has a relatively good aerodynamic shape and adjustments are limited. Therefore, to achieve further aerodynamic improvements, and thereby reduce the fuel consumption and emissions, the next step for these companies should be to consider the whole truck during the aerodynamic development. In order to do this, a co-operation between the tractor and trailer manufacturers is recommended and communication between these two should be established.
- The advantage if the tractor and the trailer were to be developed together especially applies to the interface between the cab and the trailer front, but also between the chassis and trailer underbody. A mutual development would make it possible to optimize the integration of these components, which would improve the flow transition and thereby improve both the undercarriage flow and the base flow.

6.1 Recommendations

Continuing work from here on should be to optimize the devices to see if further improvements can be achieved. For example, different angles and lengths of the plates in *Frame extension* and heights of the side skirts would be recommended to test. In addition, the devices that have been combined need to be adapted to each other to obtain the optimal flow.

$k - \varepsilon$ turbulence model is another commonly used turbulence model in the automotive industry, it would therefore be interesting to repeat the simulations with this model and compare the results. Naturally, the results of CFD simulations need to be verified with experimental data, such as wind-tunnel test, to ensure reliability of the results.

This project has only involved simulations around a Volvo FH-tractor and a standard box-trailer. Hence, the continuing work should include other types of trailers to see the efficiency of the trailer devices on different truck configurations. To verify the importance of developing tractor and trailer together it is also recommended to involve adjustments on the tractor when adding trailer devices.

It is important, from a safety aspect, to study the impact on the stability of the truck when using the different devices. To some extent, they increase the exposed frontal area of the truck, seen from the wind direction's perspective, and heavy cross-winds can thus have a negative influence on the stability of the truck, as more air hits the trailer surface and increase the side forces.

Even though there are many devices on the market today, they are not very common on the road. Next step should therefore involve further analysis of cost efficiency and user compatibility to increase the usage of the devices.

References

[1] Doe's effort to reduce aerodynamic drag through joint experiments and computations. *SAE, 2005-01-3511*, 2005.

[2] Volvo 3P/CVL. Optifuel lab - demotruck: Fuel economy results. Technical report, Volvo 3P, 2009.

[3] CD-Adapco. *STARCCM+ Manual*, version 4.06.011 edition.

[4] Meshing Research Corner. http://www.andrew.cmu.edu/user/sowen/survey/tetsurv.html, accessed 11 May 2010.

[5] L. Davidson. An introduction to turbulence models. 2003.

[6] Volvo Trucks global homepage. www.volvo/trucks/global/en-gb/home.htm, accessed 23 February 2010.

[7] Don Bur's homepage. www.donbur.co.uk/index.shtml, accessed 16 Mars 2010.

[8] W Seay J.Bledsoe, D. Landman and R Wood. Understanding practical limits to heavy truck drag reduction. *SAE, 2009-01-2890*, 2009.

[9] J. Leuschen and K.R. Cooper. Full-scale wind tunnel tests of production and prototype, second-generation aerodynamic drag-reducing devices for tractor-trailers. *SAE, 2006-01-3456*, 2006.

[10] S. Kandasamy H. Cheng R.Lietz, S. Mallick. Exterior airflow simulations using a lattice boltzmann approach. *SAE, 2002-01-0596*, 2002.

[11] R. Schoon and F.P. Pan. Practical devices for heavy truck aerodynamic drag reduction. *SAE, 2007-01-1781*, 2007.

[12] Paul Schreier. Modelling: Aerodynamics, turbulent times. Scientific computing world, June/July 2010.

[13] H K Versteeg and W Malalasekera. *An Introduction to Computational Fluid Dynamics - The Finite Volume Method*. Pearson Education Limited, 2nd edition, 2007.

[14] Frank M. White. *Fluid Mechanics*. McGraw-Hill, 5th edition, 2005.

[15] R.M. Wood. Impact of advanced aerodynamic technology on transportation energy consumption. *SAE, 2004-01-1306*, 2004.

Appendix

A Mesh Settings by Part

Table 21: Mesh settings for the tractor

Part	**Minimun size (mm)**	**Target size (mm)**	**No. of prism layers**	**Thickness Near Wall (mm)**	**Layer Thick-ness (mm)**
Cab floor	14	28	6	0,025	1,6
Cab rear	14	28	6	0,025	1,6
Cab Dir-lights	3,5	7	6	0,025	1,6
Cab Door-handles	3,5	7	6	0,025	1,6
Cab globertrotter	3,5	7	6	0,025	1,6
Cab grille	3,5	7	6	0,025	1,6
Cab handles	3,5	7	6	0,025	1,6
Cab round-edges	3,5	7	6	0,025	1,6
Cab side-mirrors	3,5	7	6	0,025	1,6
Cab lights	3,5	7	6	0,025	1,6
Cab wipers	1,75	3,5	6	0,025	1,6
Cab ext	7	14	6	0,025	1,6
Cab air-intake	7	14	6	0,025	1,6
Cab foot-steps	7	14	6	0,025	1,6
Cab roof-defl	7	14	6	0,025	1,6
Cab side-defl	7	14	6	0,025	1,6
Cab side-windows	7	14	6	0,025	1,6
Cab sun-visor	7	14	6	0,025	1,6
Cab windshield	7	14	6	0,025	1,6
Cab windshield sealing	7	14	6	0,025	1,6
Chassis engine	14	28	2	0,5	1
Chassis Fairings	7	14	2	0,5	1
Chassis front	7	14	2	0,5	1
Chassis front wheels	7	14	6	0,025	1,6
Chassis middle	7	14	2	0,5	1
Chassis rear	14	28	2	0,5	1
Chassis rear wheels	7	14	6	0,025	1,6
Cool-CAC-sides	7	14	2	0,5	1
Cool-coolpack	7	14	2	0,5	1
Cool-fan	7	14	2	0,5	1
Cool-RAD-sides	7	14	2	0,5	1
GMV CAC_in	7	14	2	0,5	1
GMV CAC_out	7	14	2	0,5	1
GMV COND_in	7	14	2	0,5	1
GMV COND_out	7	14	2	0,5	1
GMV RAD_in	7	14	2	0,5	1
GMV RAD_out	7	14	2	0,5	1

Table 22: Mesh settings for the trailer

Part	Minimun size (mm)	Target size (mm)	No. of prism layers	Thickness Near Wall (mm)	Layer Thickness (mm)
Trailer Bottom	14	28	2	0,5	1
Trailer mudwing1	7	28	2	0,5	1
Trailer mudwing 2 and 3	7	28	2	0,5	1
Trailer sides	7	56	6	0,025	1,6
Trailer sidoskydd	14	28	2	0,5	1
Trailer Top	28	56	6	0,025	1,6
Trailer Wheels 1	7	14	6	0,025	1,6
Trailer Wheels 2	7	14	6	0,025	1,6
Trailer Wheels 3	7	14	6	0,025	1,6
Tunnel Ground	448	896	2	1	3
Tunnel Inlet	448	896	-	-	-
Tunnel Outlet	448	896	-	-	-
Tunnel Roof	448	896	-	-	-
Tunnel Side Wall 1	448	896	-	-	-
Tunnel Side Wall 2	448	896	-	-	-

Table 23: Mesh settings for the devices

Device	Minimun size (mm)	Target size (mm)	No. of prism layers	Thickness Near Wall (mm)	Layer Thickness (mm)
Sealed gap	7	14	6	0,025	1,6
Vortex stabilizer	7	28	6	0,025	1,6
Gap fairing	7	28	6	0,025	1,6
Side plates	7	28	6	0,025	1,6
Base plates	7	28	6	0,025	1,6
Frame extension	7	28	6	0,025	1,6
Basedrop	7	56	6	0,025	1,6
Side skirts	7	28	6	0,025	1,6
Smooth underbody	14	28	2	0,5	1
Teardrop	28	56	6	0,025	1,6

Table 24: Mesh settings for the refinement boxes

	Customize isotropic size (mm)
VR1	112
VR2	224
VR3	448
VRblw	56

Figure 54: Refinement boxes

Table 25: Amount of cells for the different cases

Case	**No. of million cells**
Reference	41,8
Sealed gap	40,0
Vortex stabilizer	42,1
Gap fairing	42,1
Side plates	41,9
Base plates	41,9
Frame extension	42,1
Basdrop	41,7
Side skirts	42,8
Smooth underbody	40,1
Sealed wheels	42,7
Teardrop	41,8
Frame extension and Side skirts	43,1
Gap fairing and Frame extension	42,3
Gap fairing, Frame extension and Side skirts	43,4
Teardrop and Frame extension	42,0
Teardrop and Side skirts	42,9
Gap fairing, Frame extension, Side skirts and Teardrop	43,4

B Solver settings

- *Segregated flow*
  - Velocity
    - Under-realxation = 0.5
    - AMG Linear Solver
      - Flex Cycle
      - Gauss-Seidel scheme
  - Pressure
    - Under-relaxation = 0.15
    - AMG Linear Solver
      - Fixed Cycle
      - Gauss-Seidel scheme
- *K-Omega Turbulence*
  - Under-realxation = 0.7
  - AMG Linear Solver
    - Flex Cycle
    - Gauss-Seidel scheme
- *K-Omega Turbulent Viscosity*
  - Under-realxation = 1.0

C Drawings

Reference

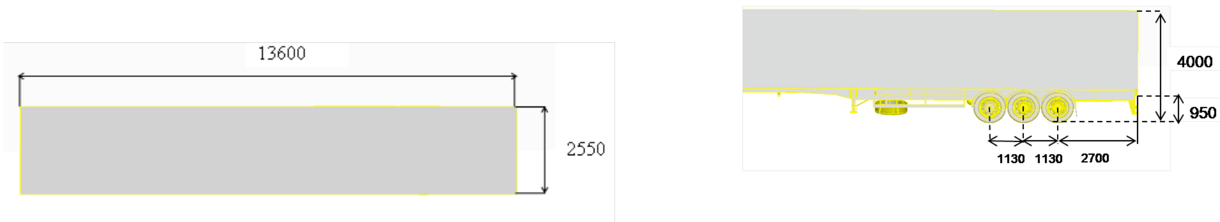

Figure 55: Reference trailer - top and side view, measures in mm

Vortex stabilizer

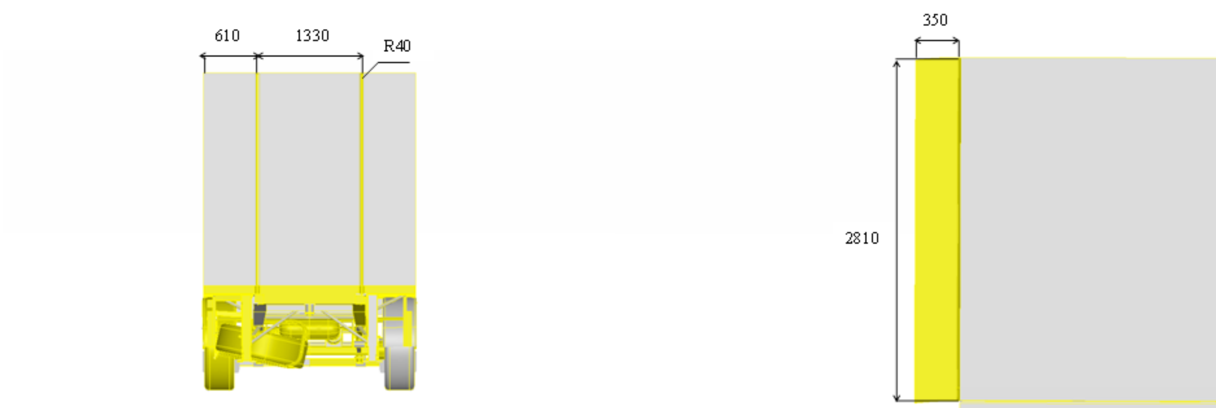

Figure 56: Vortex stabilizer - front and side view, measures in mm

Base plates

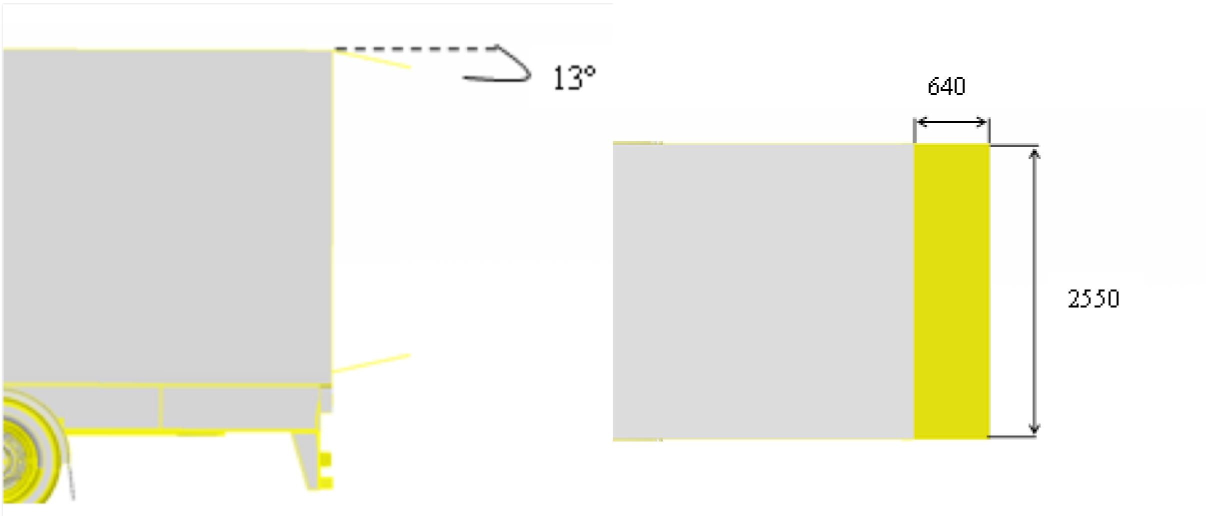

Figure 57: Base plates - side and top view, measures in *mm*

Side plates

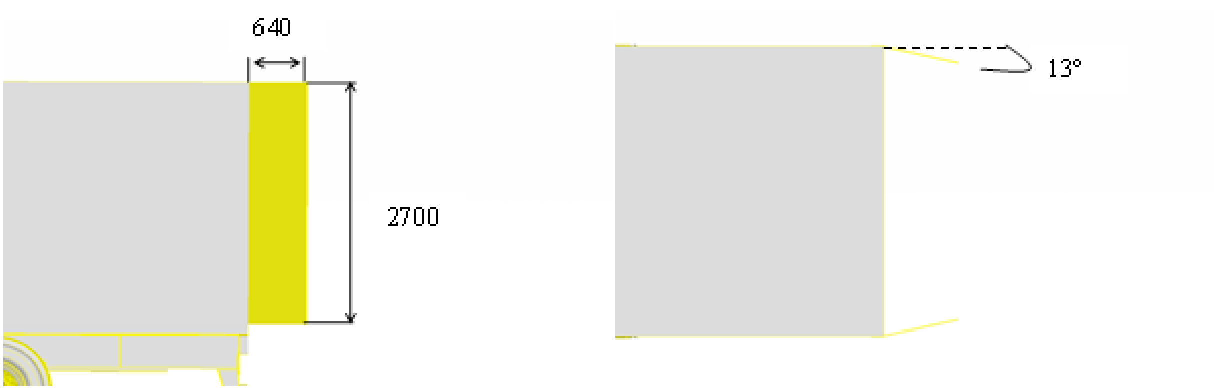

Figure 58: Side plates - side and top view, measures in *mm*

Side skirts

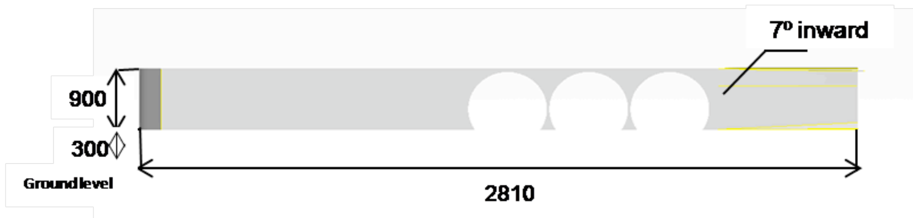

Figure 59: Sideskirts - side view, measures in mm

Teardrop

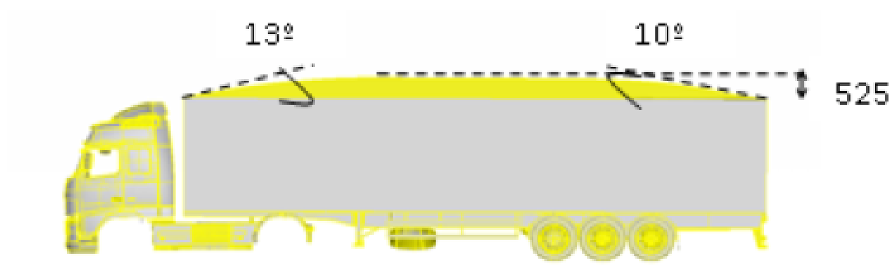

Figure 60: Teardrop - sideview, measures in mm

Wind-tunnel / Computational Domain

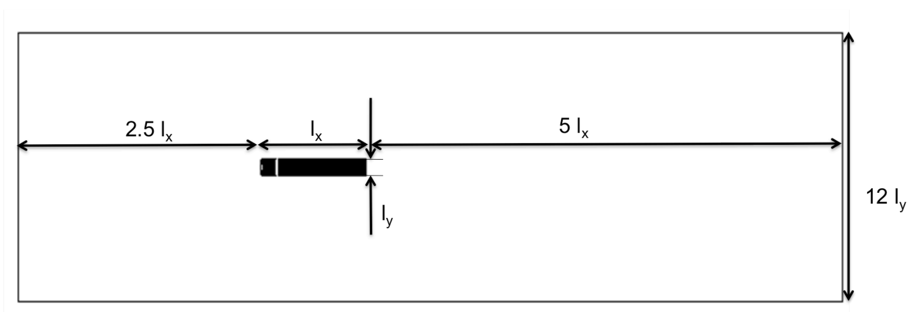

Figure 61: Wind-tunnel seen from above. Hight of the tunnel is equal to five times the truck height. Measures in m: $135 \times 36 \times 20$ $[x, y, z]$

D Pictures

D.1 Sealed gap

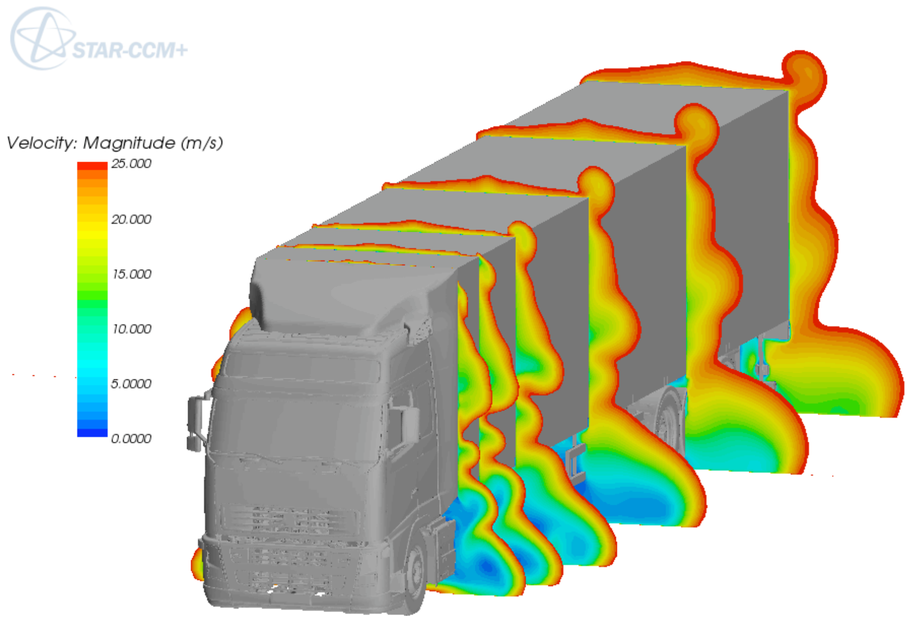

Figure 62: Velocity magnitude in different x-planes along trailer, 0° yaw

D.2 Vortex stabilizer

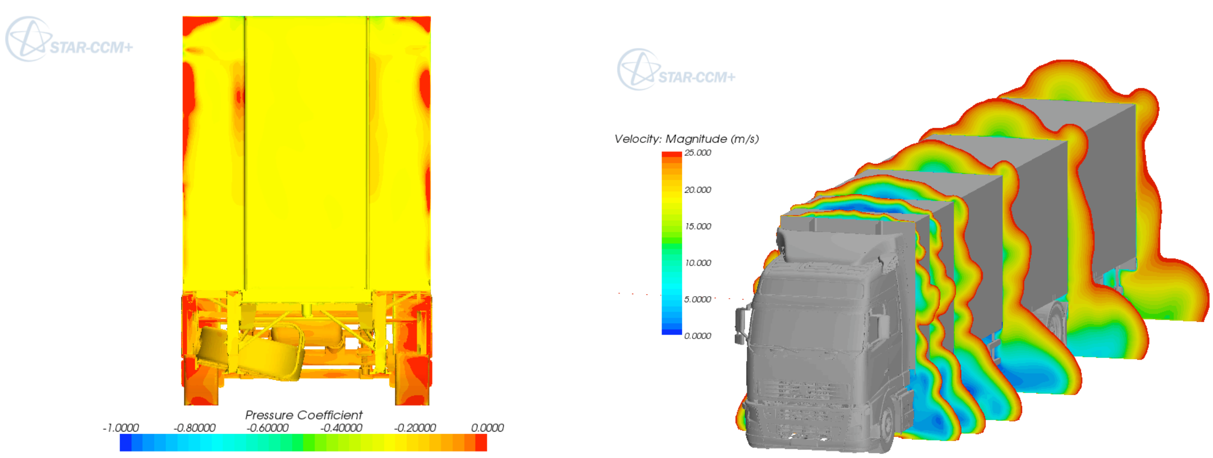

Figure 63: Pressure coefficient at trailer front and velocity magnitude in x-planes along trailer, 0° yaw

D.3 Base plates

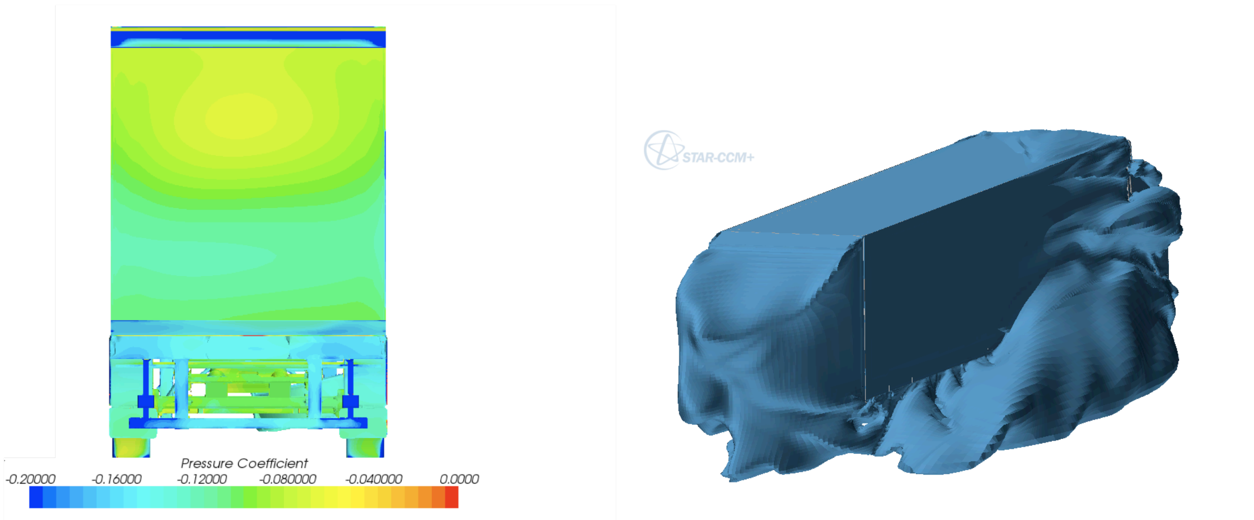

(a) Pressure coefficient displayed on the trailer back, 0° yaw (b) Iso surface of total pressure equal to zero at the rear of the trailer, 5° yaw

Figure 64: Base plates

D.4 Smooth underbody

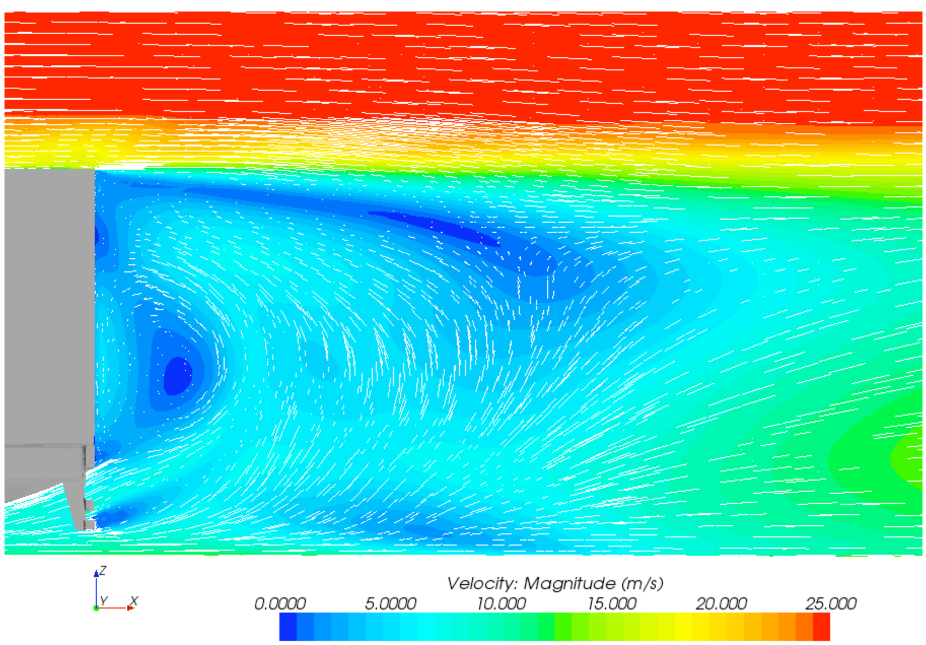

Figure 65: Velocity magnitude displayed in the symmetry plane, 0° yaw

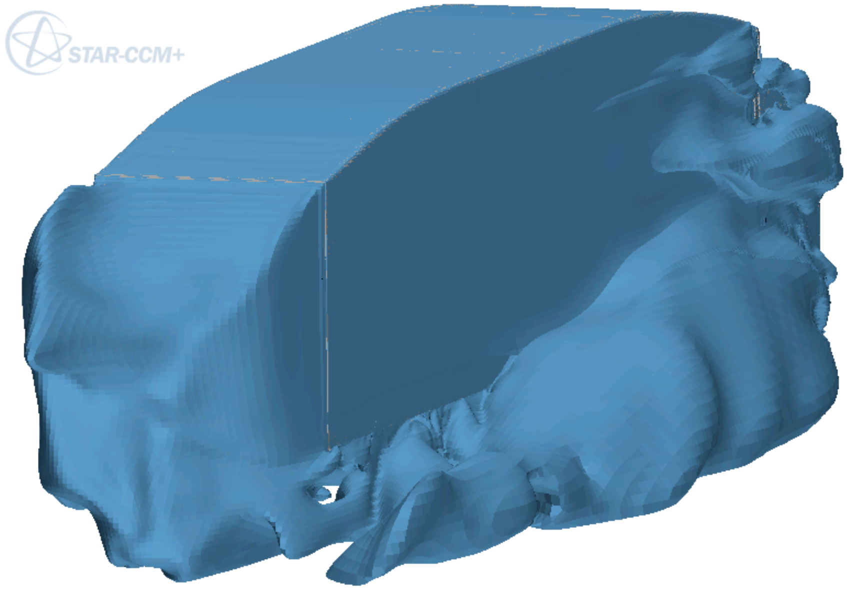

Figure 67: Iso surfaces of total pressure equal to zero, 5° yaw

D.5 Teardrop

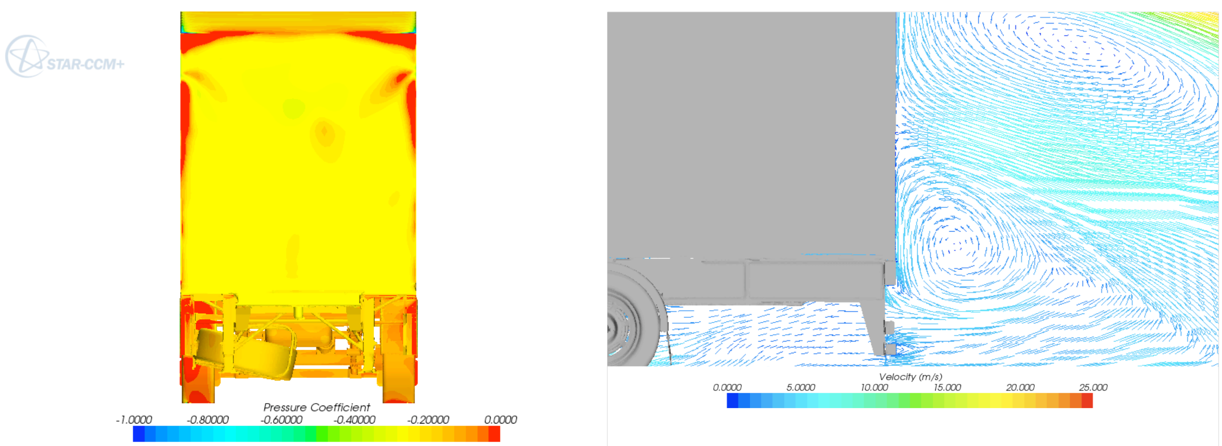

Figure 66: Pressure coefficient at the trailer front and velocity vectors at the rear of the trailer, 0° yaw

D.6 Basedrop

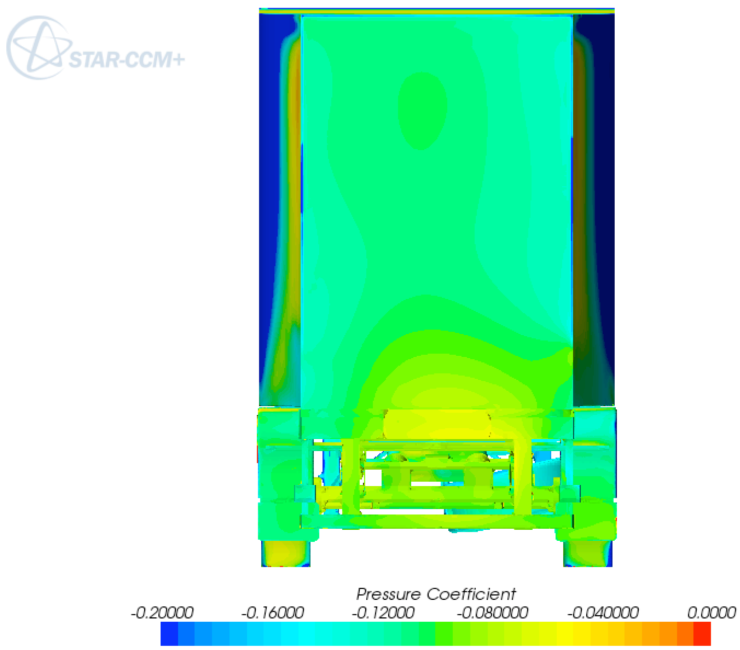

Figure 68: Pressure distribution at the trailer back, 0° yaw

D.7 Gap fairing and Frame extension

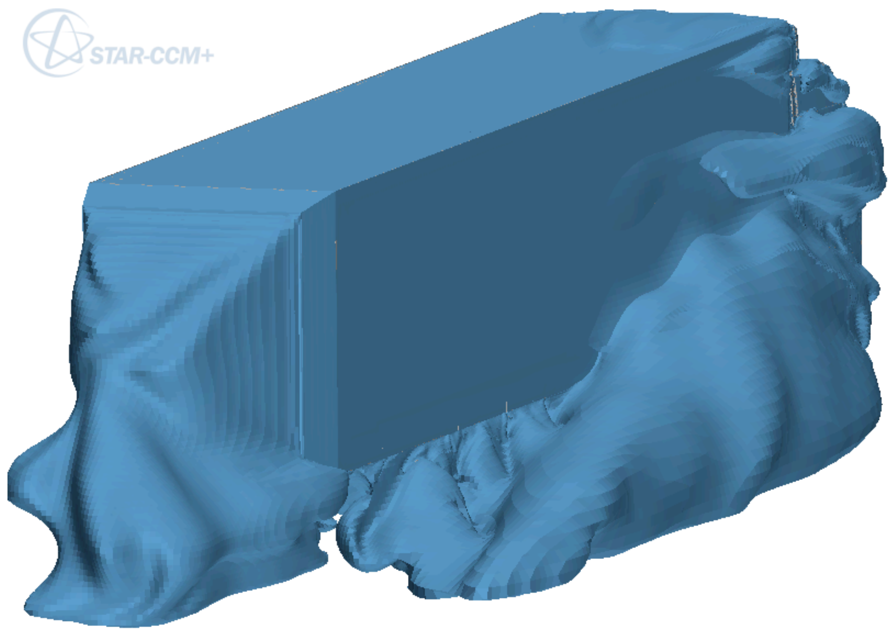

Figure 69: Iso surfaces of total pressure equal to zero, 5° yaw

D.8 Teardrop and Frame extension

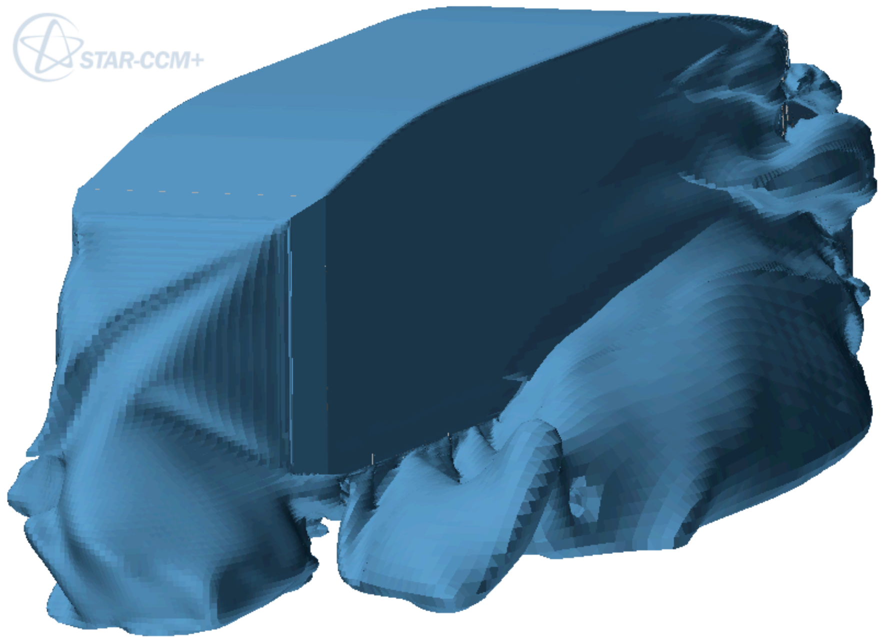

Figure 70: Iso surfaces of total pressure equal to zero, 5° yaw

D.9 Teardrop and Side skirts

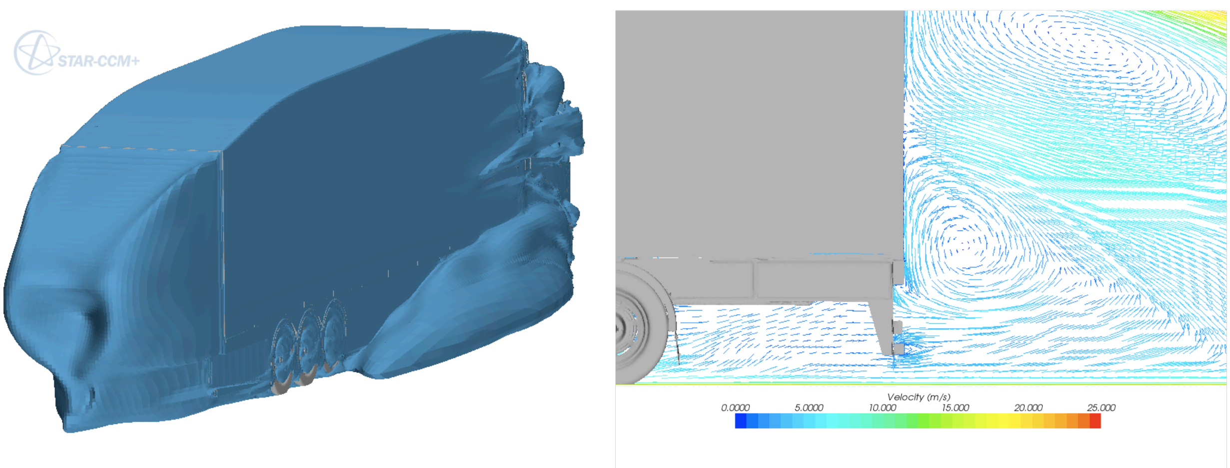

Figure 71: Iso surface from above and velocity vectorsat the rear of trailer, 5° and 0° yaw respectively

D.10 Gap fairing, Frame extension, Side skirts and Teardrop

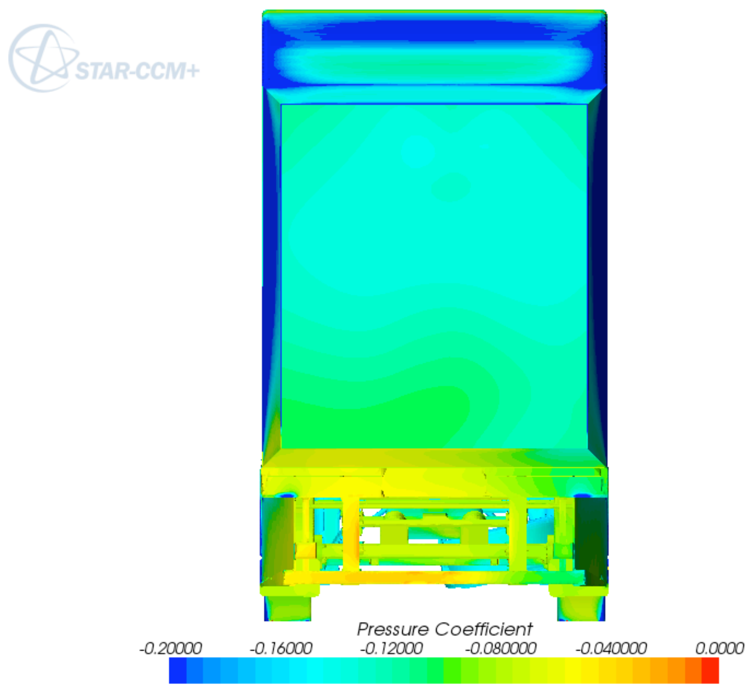

Figure 72: Pressure distribution at the trailer back, 0° yaw